AD-A067 664 ARMY MISSILE RESEARCH AND DEVELOPMENT COMMAND REDSTO--ETC F/G 20/1
ACOUSTICAL SPECKLE INTERFEROMETRY.(U)
MAR 79 J A SCHAEFFEL

UNCLASSIFIED DRDMI-T-79-39 NL

1 OF 2
ADA 067664

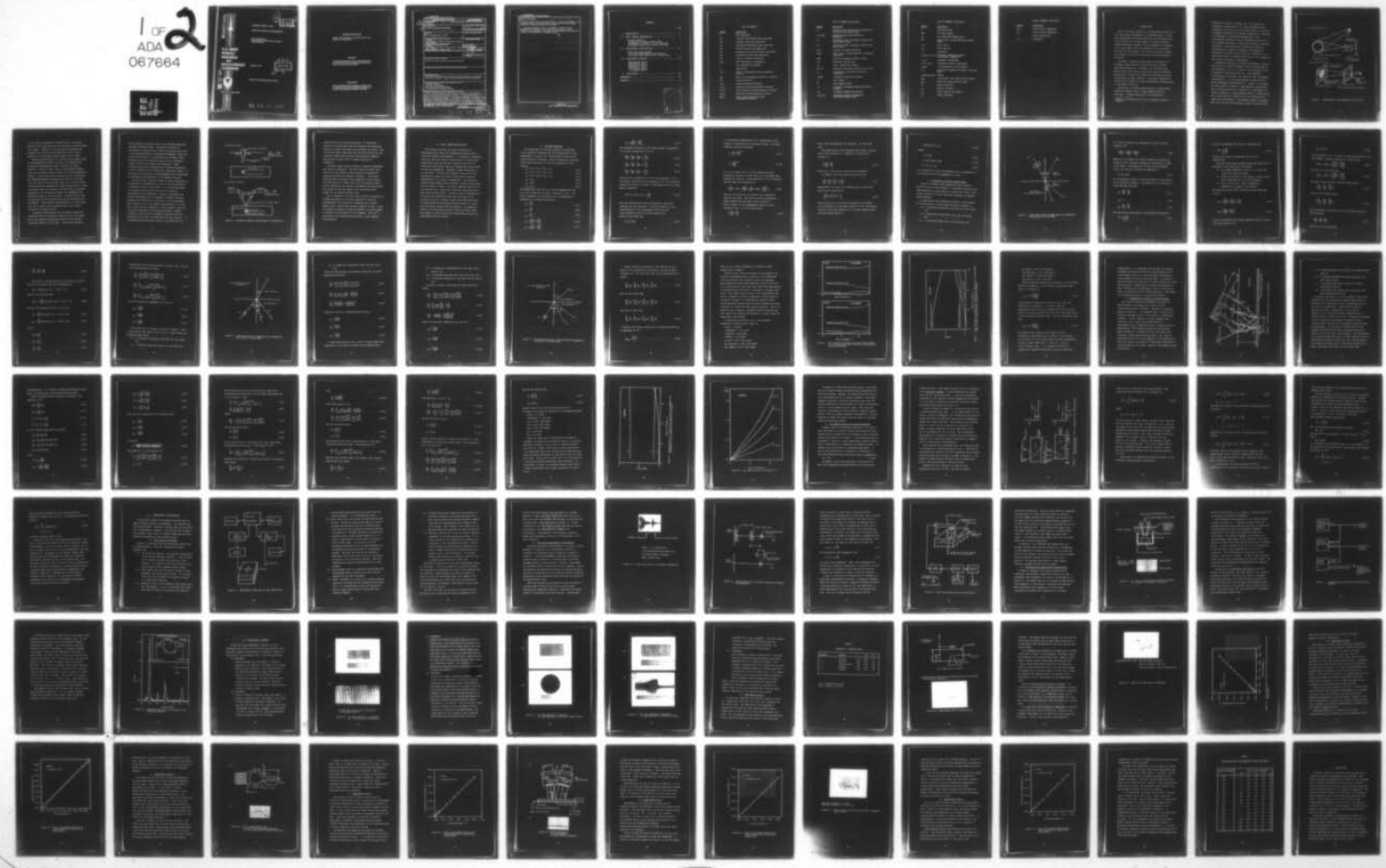


A
664

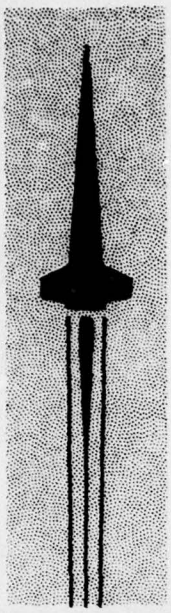

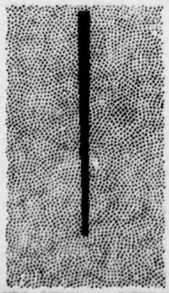

(12) NW LEVEL II

TECHNICAL REPORT T-79-39

ACOUSTICAL SPECKLE INTERFEROMETRY

John Arnold Schaeffel, Jr.
Ground Equipment and Missile Structures Directorate
Technology Laboratory

U.S. ARMY MISSILE RESEARCH AND DEVELOPMENT COMMAND

Redstone Arsenal, Alabama 35809

22 MARCH 1979

Approved for public release; distribution unlimited

DISPOSITION INSTRUCTIONS

DESTROY THIS REPORT WHEN IT IS NO LONGER NEEDED. DO NOT RETURN IT TO THE ORIGINATOR.

DISCLAIMER

THE FINDINGS IN THIS REPORT ARE NOT TO BE CONSTRUED AS AN *OFFICIAL DEPARTMENT OF THE ARMY POSITION UNLESS SO DESIG-*NATED BY OTHER AUTHORIZED DOCUMENTS.

TRADE NAMES

USE OF TRADE NAMES OR MANUFACTURERS IN THIS REPORT DOES NOT CONSTITUTE AN OFFICIAL INDORSEMENT OR APPROVAL OF THE USE OF SUCH COMMERCIAL HARDWARE OR SOFTWARE.

UNCLASSIFIED

SECURITY CLASSIFICATION OF THIS PAGE (When Data Entered)

REPORT DOCUMENTATION PAGE		READ INSTRUCTIONS BEFORE COMPLETING FORM
1. REPORT NUMBER (17) DRDMI-T-79-39	2. GOVT ACCESSION NO.	3. RECIPIENT'S CATALOG NUMBER
4. TITLE (and Subtitle) (6) ACOUSTICAL SPECKLE INTERFEROMETRY		5. TYPE OF REPORT & PERIOD COVERED (9) Technical rept.
		6. PERFORMING ORG. REPORT NUMBER
7. AUTHOR(s) (10) John Arnold Schaeffel, Jr.		8. CONTRACT OR GRANT NUMBER(s)
9. PERFORMING ORGANIZATION NAME AND ADDRESS Commander US Army Missile Research and Development Command Attn: DRDMI-TL Redstone Arsenal, Alabama 35809		10. PROGRAM ELEMENT, PROJECT, TASK AREA & WORK UNIT NUMBERS
11. CONTROLLING OFFICE NAME AND ADDRESS Commander US Army Missile Research and Development Command Attn: DRDMI-TI Redstone Arsenal, Alabama 35809		12. REPORT DATE (11) 22 March 1979 13. NUMBER OF PAGES ~~107~~ (12) 130
14. MONITORING AGENCY NAME & ADDRESS (if different from Controlling Office)		15. SECURITY CLASS. (of this report) Unclassified
		15a. DECLASSIFICATION/DOWNGRADING SCHEDULE

16. DISTRIBUTION STATEMENT (of this Report)

Approved for public release; distribution unlimited

17. DISTRIBUTION STATEMENT (of the abstract entered in Block 20, if different from Report)

18. SUPPLEMENTARY NOTES

This report was prepared as a thesis in partial fulfillment of the requirements for the degree of Master of Science submitted to Auburn University.

19. KEY WORDS (Continue on reverse side if necessary and identify by block number)

Pulse-echo scanning
Continuous wave scanning
Acoustical Speckle Interferometry
Interferometric Displacement Analysis

20. ABSTRACT (Continue on reverse side if necessary and identify by block number)

When a continuous wave or pulsed beam of ultrasound is scanned over an object an echo from the object may be detected. If the echo has a random variation in amplitude versus position of the beam, the resulting variation is referred to as acoustical speckle. An analysis is presented for using acoustical speckle to determine displacements on the surface or interior to an object. Two experimental configurations, pulse-echo scanning and continuous wave scanning, are treated in the verification of the analysis. Six experiments are conducted using numerical cross-correlation analysis to verify the hypothesis that (Continued)

Next Page

DD FORM 1 JAN 73 1473 EDITION OF 1 NOV 65 IS OBSOLETE

UNCLASSIFIED

SECURITY CLASSIFICATION OF THIS PAGE (When Data Entered)

ABSTRACT (Concluded)

acoustical speckle interferometry may be used to determine displacements. The experiments indicate that displacements as small as the discrete sampling interval of the ultrasonic beam can be predicted.

Pulse-echo scanning is found to be sensitive to motion in three-dimensions while continuous wave (CW) scanning is sensitive to motion primarily in two-dimensions. Both methods of beam scanning produce excellent results for interferometric displacement analysis.

CONTENTS

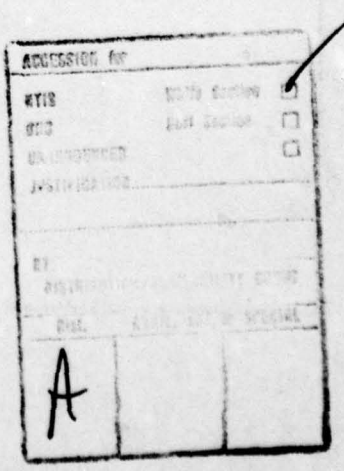

LIST OF SYMBOLS

Symbol	Definition
A_i	wave amplitude
AiL	incident longitudinal wave amplitude
AiS	incident shear wave amplitude
ArL	reflected longitudinal wave amplitude
ArS	reflected shear wave amplitude
AtL	transmitted longitudinal wave amplitude
AtS	transmitted shear wave amplitude
A/D	analog to digital conversion
$A(\omega)$	wave amplitude at frequency ω
c	wave propagation velocity
C	capacitance
c_{iL}	media i longitudinal wave propagation velocity
c_{iS}	shear wave propagation velocity in media i
CW	continuous wave
$C(\tau)$	cross-correlation function
$C'(\tau)$	difference cross-correlation function
$C''(\tau)$	least squares cross-correlation function
$C_D(L)$	discrete cross-correlation function
$C_D^*(L)$	least squares discrete cross-correlation function

LIST OF SYMBOLS (Continued)

Symbol	Definition
D	distance from liquid-solid interface to reflecting-scattering layer
D_i, d_i, d_i^*	distances over which waves are propagated
D_L	scattering layer intercept distance for longitudinal waves
D_S	scattering layer intercept distance for shear waves
D/A	digital to analog conversion
Eapp	open circuit voltage applied to transmit transducer
Eout	receiver transducer output voltage
f(x)	arbitrary function of x
G_i	Lame' constant for media i
h(x,z)	arbitrary continuous function of x and z
h_i	distance for locating a receiving transducer
$\hat{i}, \hat{j}, \hat{k}$	cartesian system unit vectors
k	wave number
$\bar{k}$	wave number vector
L,r	integers in discrete cross-correlation analysis
Δn	increment between scan points
n_x, n_y, n_z	direction cosines in cartesian coordinate system $\hat{i}, \hat{j}, \hat{k}$

LIST OF SYMBOLS (Continued)

Symbol	Definition
$\bar{r}$	position vector
RMS	root mean square
S_i	wave amplitude energy ratio
S_i^*	square root of wave amplitude energy ratio
t, t_i	time, time i
Δt_i	time interval i
R	resistance
u_x, u_y, u_z, u, v, w	cartesian coordinate system displacement components
x, y, z	cartesian coordinates
x', x'', x_a, x_b	transducer scanner coordinates
$\Delta x, \Delta y$	x,y deformation of test object
Zij	acoustical impedance of media i for wave type j
$\alpha, \beta, \epsilon, \eta, \mu, \Delta, \psi$	angles
αCL	longitudinal wave type critical angle
αCS	shear wave type critical angle
ϕ	scalar potential
ρi	density of media i
λi	Lame' constant for media i
$\bar{\psi}$	vector potential

LIST OF SYMBOLS (Continued)

Symbol	Definition
σ_{ij}	stress tensor components
ϵ_{ij}	strain tensor components
τ	signal phase shift
ω, w	frequency

I. INTRODUCTION

One of the major objectives in experimental mechanics is the displacement measurement in a deformable body. In the past, measurements of such deformation have been restricted to the surface of the body, however for many structures, surface deformation analysis is quite adequate as evidenced by the many reports that have appeared in the literature over the past two decades. As structural analysis becomes more complex, the need for examining internal deformation has arisen.

Ultrasonic inspection using beams of ultrasound is a technique growing rapidly to fill the needs of modern experimental mechanics. Ensminger [1]* documents many modern applications dealing with topics such as thickness measurements, inspection of metals and non-metals and the determination of bond integrity. Ultrasonic inspection is further being extended to tissue examinations and bone scans in the medical field [2].

Essentially all modern applications of ultrasound for inspection purposes seek to image anomalies within a structure. A modern application of ultrasound for

---

* Numbers in brackets refer to the references listed on page 89.

deformation analysis is through the use of acoustical holographic interferometry [3]. This technique uses a reference and object beam of ultrasound similar to optical holography to produce an acoustical hologram of a structure in a deformed and undeformed configuration. The interferogram, recorded using an oscilloscope and film, is then reconstructed using a laser system similar to optical holography. The reconstructed interference effect is interpreted as in optical holographic interferometry. Although the technique suffers from poor resolution, it is significant since it represents one of the first attempts to make internal deformation measurements.

Holographic techniques for making measurements require a high degree of vibration isolation since the magnitude of the measurements are on the order of the wavelength of the illuminating light source used [4]. Laser speckle interferometry, being much less sensitive than holographic interferometry, is a technique growing in popularity for making deformation measurements [5]. Figure 1 illustrates the basic method for making a laser speckle interferogram. When a diffuse surface of a structure is illuminated with coherent radiation, a grainy speckle effect is imaged by the eye or film plane of a camera due to the interference of light from the structure. This speckle effect is enhanced when the structure has microscopic surface irregularities.

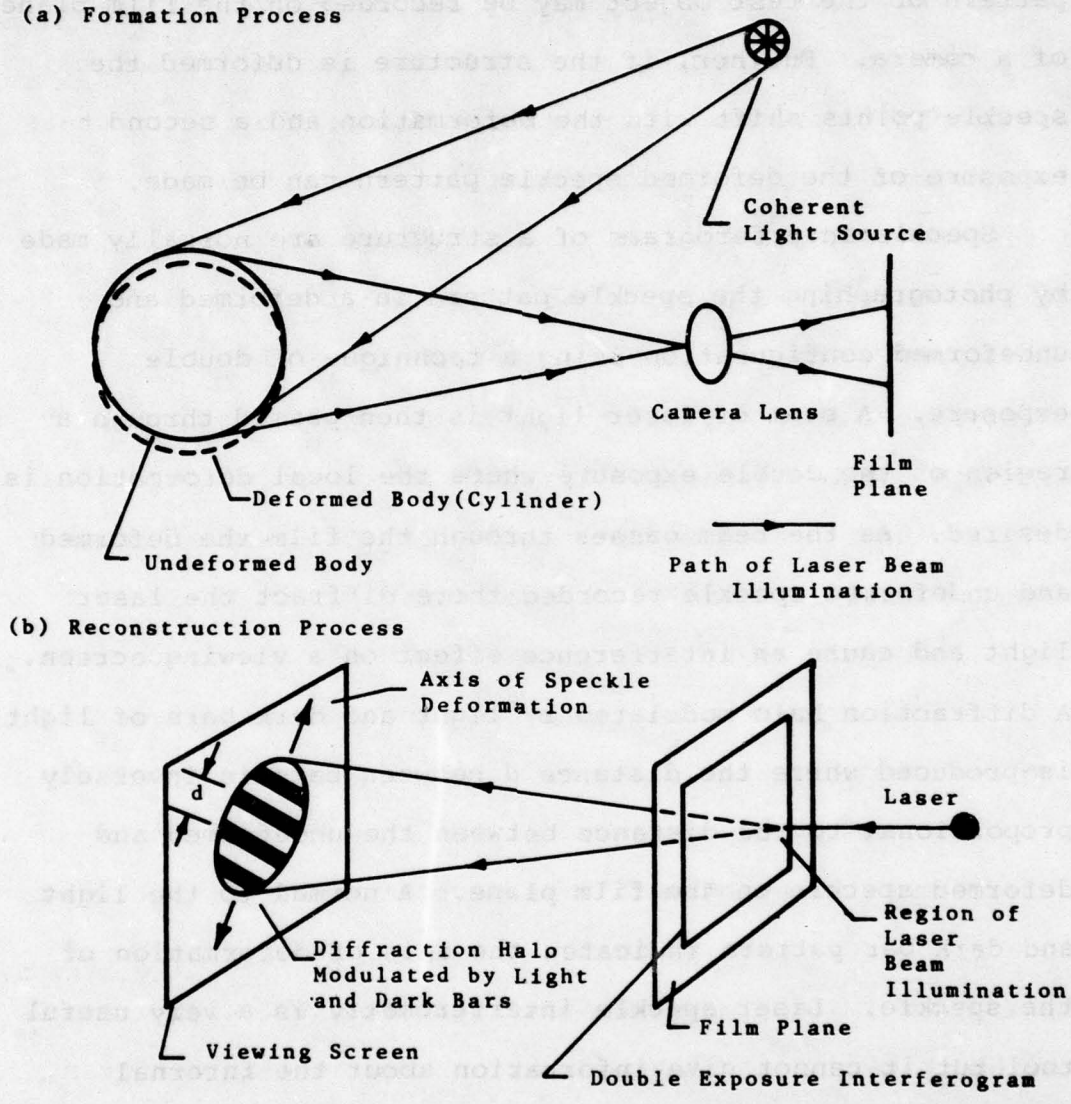

Figure 1. Laser Speckle Interferometry Configuration

If the optical configuration remains fixed, the speckle pattern of the test object may be recorded on the film plane of a camera. Further, if the structure is deformed the speckle points shift with the deformation and a second exposure of the deformed speckle pattern can be made.

Speckle interferograms of a structure are normally made by photographing the speckle pattern in a deformed and undeformed configuration using a technique of double exposure. A beam of laser light is then passed through a region of the double exposure where the local deformation is desired. As the beam passes through the film the deformed and undeformed speckle recorded there diffract the laser light and cause an interference effect on a viewing screen. A diffraction halo modulated by light and dark bars of light is produced where the distance d between bars is inversely proportional to the distance between the undeformed and deformed speckle on the film plane. A normal to the light and dark bar pattern indicates the axis of deformation of the speckle. Laser speckle interferometry is a very useful tool but it cannot give information about the internal deformation of opaque solids.

In speckle interferometry the film plane records the amplitude variation across the surface of the test object due to the multiple interference effect of the various scattering points on the surface. Ultrasound provides a

direct analogy to light in that it too has both amplitude and phase characteristics. The direct extension of substituting a sound wave for light is an obvious one since it was first performed in acoustical holography. When the surface of an object is irradiated with ultrasound small irregularities in the surface, often in the microscopic regime, reflect and transmit the ultrasound. These irregularities may be recorded with a receiving transducer to give a mapping of the surface over some small region. If the surface is displaced, the displacement can be determined by examining the displacement of the mapping function.

One of the most important facets of using ultrasound for interferometric measurements is that it has the capability to penetrate into the test object. If a scattering region of ultrasound exists within the structure then its displacement can be predicted. Figure 2 illustrates two possible configurations for mapping the random ultrasonic interference effects from a structure. In the pulse-echo mode, usually a 1.0-4.0 μs pulse of ultrasound of 1.0-10.0 MHz is sent from the transducer to the structure. When the ultrasound encounters the structure-acoustical couplant interface, a portion of the energy is reflected from the interface and the rest is transmitted into the material. If an anomaly below the surface exists, a reflected echo is

(a) Pulse-Echo Mode

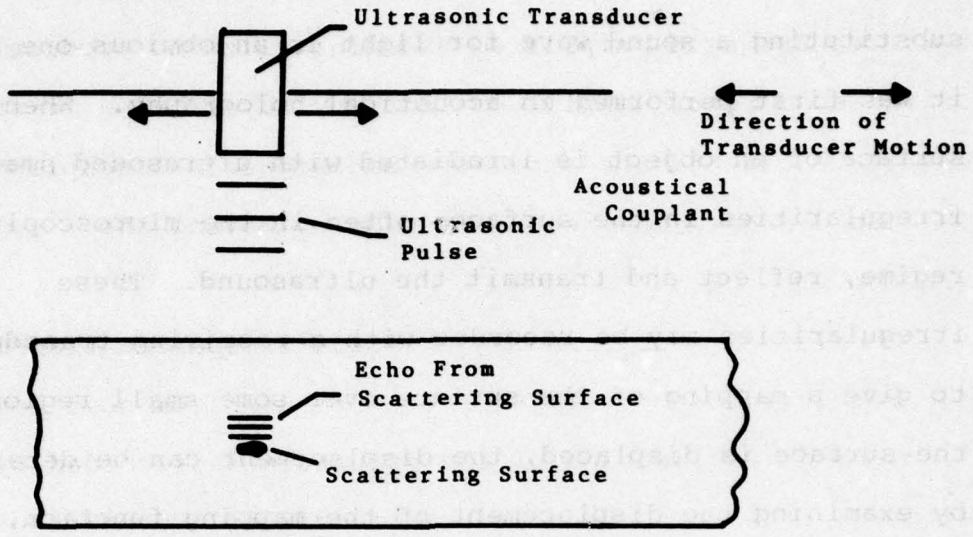

(b) Continuous Wave Mode

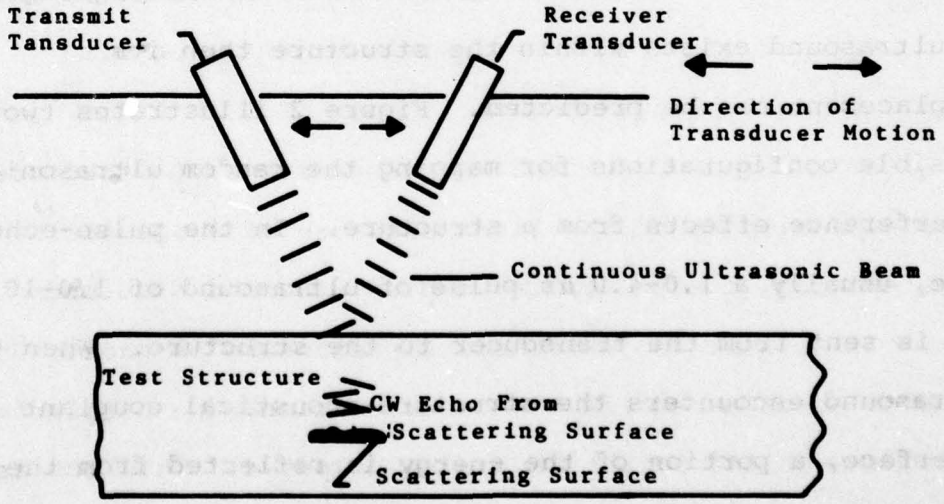

Figure 2. Acoustical Speckle Interferometry Configuration

produced from this scattering surface. In pulse-echo scanning the return echo from the interface and scattering surfaces is gated, amplified and digitalize to produce a map of the echo return amplitude from any layer below or at the interface between the structure and acoustical couplant. The map over a plane region is made by moving the transducer.

Continuous mode scanning utilizes a separate transmitter and receiver transducer. The echo return from some level below or at the surface of the structure is recorded by properly orienting the receiver transducer. Continuous scanning tends to produce better mappings of echo returns than pulse-echo for reasons which will be explained later. As the transmitter and receiver transducers are moved across the surface of the test object their orientation with respect to one another remains fixed.

After a mapping of the echo return from the structure is recorded analogous to the first exposure of a speckle interferogram, the structure is displaced and a second mapping like a second laser speckle exposure is made. Using the process of numerical cross-correlation, the displacement of regions on the structure can be computed. This too is analogous to the reconstruction process in laser speckle interferometry.

II. BASIC PROBLEM DESCRIPTION

This section presents the theory necessary for understanding the basic wave propagation process used in acoustical speckle interferometry. In ultrasonic inspection there are four basic types of wave motion of interest [6]. Longitudinal waves are the most important wave form in solids and liquid media which are compressional waves along the axis of propagation. Examples include sound waves in air and water. The next most important wave form is the transverse or shear wave which involve particle motion perpendicular to the axis of propagation. Low viscosity liquids cannot support shear stresses, therefore these waves are only found in solids. The third important wave form is the Rayleigh wave. These waves show both longitudinal and shear wave characteristics. Particle motion is generally in the form of an ellipse and they can only exist on the surface of a solid. Finally, there is the Lamb wave which is characterized by elliptical particle motion in a solid with two closely spaced parallel surfaces. An example is found in the vibrational motion of plate and sheet stock. The analysis in this section will concentrate primarily on longitudinal and shear waves.

2.1 The Wave Equation

The formulation of the wave equation is based upon linear elasticity coupled with the representation of the displacement of points in a continuum by the vector and scalar potential functions. Basic stress-strain relations from linear elasticity [7] form the foundation of the analysis

$$\sigma_{xx} = (2G + \lambda)\varepsilon_{xx} + \lambda(\varepsilon_{yy} + \varepsilon_{zz}) \tag{2.1}$$

$$\sigma_{yy} = (2G + \lambda)\varepsilon_{yy} + \lambda(\varepsilon_{xx} + \varepsilon_{zz}) \tag{2.2}$$

$$\sigma_{zz} = (2G + \lambda)\varepsilon_{zz} + \lambda(\varepsilon_{xx} + \varepsilon_{yy}) \tag{2.3}$$

$$\sigma_{xy} = 2G\varepsilon_{xy} \tag{2.4}$$

$$\sigma_{yz} = 2G\varepsilon_{yz} \tag{2.5}$$

$$\sigma_{zx} + 2G\varepsilon_{zx} \tag{2.6}$$

These equations relate the σ_{ij} stress components to the ϵ_{ij} strain components and Lame' constants λ and G. The strain components are related to the u_i displacement components in a cartesian system by

$$\varepsilon_{xx} = \frac{\partial u_x}{\partial x} \tag{2.7}$$

$$\varepsilon_{yy} = \frac{\partial u_y}{\partial y} \tag{2.8}$$

$$\varepsilon_{zz} = \frac{\partial u_z}{\partial z} \tag{2.9}$$

$$\varepsilon_{xy} = \frac{1}{2}\left\{\frac{\partial u_x}{\partial y} + \frac{\partial u_y}{\partial x}\right\} \tag{2.10}$$

$$\varepsilon_{zx} = \frac{1}{2}\left\{\frac{\partial u_z}{\partial x} + \frac{\partial u_x}{\partial z}\right\} \tag{2.11}$$

$$\varepsilon_{yz} = \frac{1}{2}\left\{\frac{\partial u_y}{\partial z} + \frac{\partial u_z}{\partial y}\right\} \tag{2.12}$$

The equations of motion in the linear theory of elasticity are listed in Equations 2.13-2.15:

$$\frac{\partial \sigma_{xx}}{\partial x} + \frac{\partial \sigma_{xy}}{\partial y} + \frac{\partial \sigma_{xz}}{\partial z} = \rho \frac{\partial^2 u_x}{\partial t^2} \tag{2.13}$$

$$\frac{\partial \sigma_{yx}}{\partial x} + \frac{\partial \sigma_{yy}}{\partial y} + \frac{\partial \sigma_{yz}}{\partial z} = \rho \frac{\partial^2 u_y}{\partial t^2} \tag{2.14}$$

$$\frac{\partial \sigma_{zx}}{\partial x} + \frac{\partial \sigma_{zy}}{\partial y} + \frac{\partial \sigma_{zz}}{\partial z} = \rho \frac{\partial^2 u_z}{\partial t^2} \tag{2.15}$$

Substitution of Equations 2.7-2.12 into Equations 2.1-2.6 and further substitution into Equations 2.13-2.15 yields the equations of motion in terms of displacement which is called Navier's Equation:

$$G\nabla^2\bar{u} + (\lambda + G)\nabla(\nabla \cdot \bar{u}) = \rho \frac{\partial^2 \bar{u}}{\partial t^2} \tag{2.16}$$

With the presentation of Navier's Equation, three new equations can be introduced. The first equation is the representation of the displacement field $\bar{u}$ by the scalar potential ϕ and the vector potential $\bar{\psi}$. Wills [8] has shown that

$$\bar{u} = \nabla\phi + \nabla x\bar{\psi} \tag{2.17}$$

is a legitimate representation of a displacement field subject to conditions that continuity exists. Two other relations can now be defined:

$$C_L \equiv \left\{ \frac{\lambda + 2G}{\rho} \right\}^{1/2} \tag{2.18}$$

$$C_T \equiv \left\{ \frac{G}{\rho} \right\}^{1/2} \tag{2.19}$$

It is to be shown that c_L is the longitudinal wave propagation velocity of sound while c_T is the shear wave propagation velocity. Using Equations 2.17-2.19, Navier's Equation may now be expressed as

$$\nabla \left[C_L^2 \nabla \cdot (\nabla \phi) - \frac{\partial^2 \phi}{\partial t^2} \right] - \nabla x \left[C_T^2 \nabla x (\nabla x \bar{\psi}) + \frac{\partial^2 \bar{\psi}}{\partial t^2} \right] = 0 \tag{2.20}$$

Equation 2.20 describes the general wave propagation equation for sound. Two cases can now be considered. First consider the case when $v=w=0$, $u \neq 0$ and $\bar{u} = \bar{u}(x-ct)$ where c is the propagation velocity of the ultrasonic wave. It can be shown that:

$$C_L^2 \frac{\partial^2 u}{\partial x^2} = \frac{\partial^2 u}{\partial t^2} \tag{2.21}$$

This is the longitudinal wave equation. For this case $c=c_L$.

The second case is for transverse wave motion in which $u=w=0$, $v\neq 0$ and $\bar{u}=\bar{u}(x-ct)$. Equation 2.16 may then be written as:

$$c_T^2 \frac{\partial^2 v}{\partial x^2} = \frac{\partial^2 v}{\partial t^2} \tag{2.22}$$

where $c_T=c$. This is the transverse wave equation.

In general, the wave equation takes the form

$$\frac{\partial^2 F}{\partial x^2} + \frac{\partial^2 F}{\partial y^2} + \frac{\partial^2 F}{\partial z^2} = \frac{1}{c^2} \frac{\partial^2 F}{\partial t^2} \tag{2.23}$$

Brekhovskikh [9] states the simplest form of plane wave motion may be expressed as

$$F\left\{\frac{x\eta_x + y\eta_y + z\eta_z}{c} - t\right\} \tag{2.24}$$

where n_x, n_y, n_z are the direction cosines of the normal to the wavefront in coordinate system $\hat{i}$, $\hat{j}$, $\hat{k}$. The general solution to the wave equation for a single frequency wave omitting a phase angle is

$$A(w)\exp[i(\bar{k}\cdot\bar{r} - wt)] \tag{2.25}$$

where,

$$k = \frac{w}{c} = \frac{2\pi}{\lambda} \tag{2.26}$$

$$\bar{k} = kn_x\hat{i} + kn_y\hat{j} + kn_z\hat{k} \tag{2.27}$$

$$\bar{r} = x\hat{i} + y\hat{j} + z\hat{k} \tag{2.28}$$

It is important to note that Equation 2.25 is analogous to the expression for the propagation of light.

2.2 Propagation of Sound between Media

When an ultrasonic wave propagates from a liquid to solid or solid to liquid medium, it undergoes reflection and mode conversion to longitudinal and shear wave forms. This section presents the basic equations necessary to describe these phenomena.

A longitudinal wave propagating through a liquid media to a solid results in three waves as shown in Figure 3:

(1) a reflected longitudinal wave back into the liquid, ArL.

(2) a transmitted longitudinal wave into the solid, AtL.

(3) a transmitted shear wave into the solid, AtS.

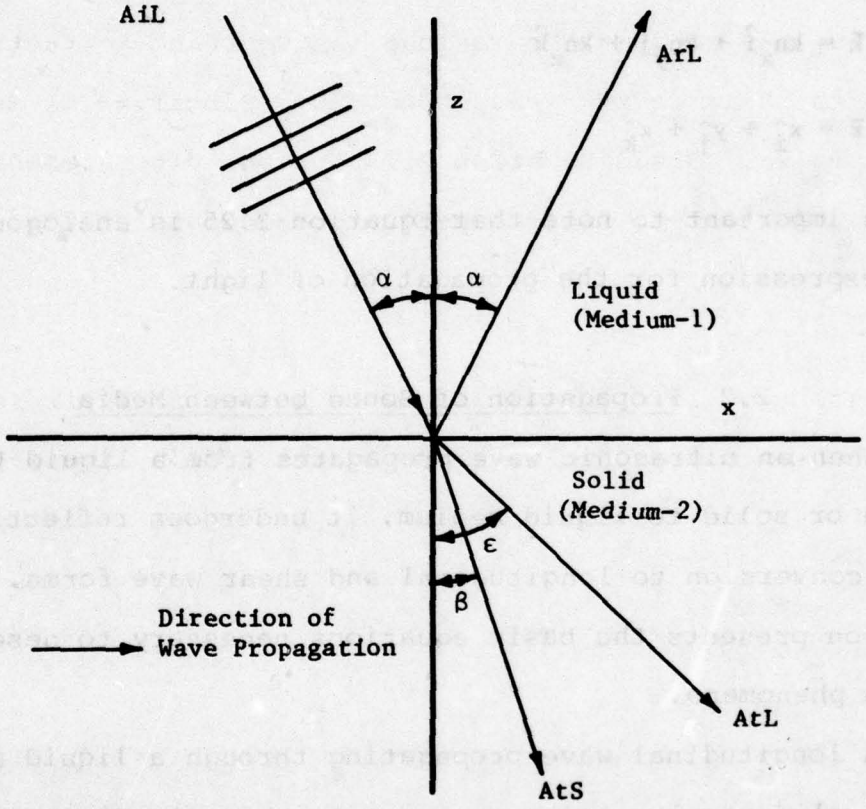

Figure 3. Longitudinal Wave of Amplitude AiL Propagating from Liquid to Solid Media

As in optics there is the equivalent of Snell's Law for acoustics [9]

$$\frac{\sin(\alpha)}{C_{1L}} = \frac{\sin(\beta)}{C_{2S}} = \frac{\sin(\varepsilon)}{C_{2L}} \tag{2.29}$$

Equation 2.29 relates the various incident and refraction angles to their respective propagation velocities of sound in the media. Given Equation 2.17 for the displacement field, the velocity field may be expressed as

$$\dot{\vec{u}} = \nabla\dot{\phi} + \nabla x\dot{\vec{\psi}} \tag{2.30}$$

As illustrated in Figure 3, the wave motion is restrained to the xz-plane for analysis. From Equation 2.30, the particle velocities have the form

$$\dot{u}_x = \frac{\partial\dot{\phi}_x}{\partial x} - \frac{\partial\dot{\psi}_y}{\partial z} \tag{2.31}$$

$$\dot{u}_y = 0 \tag{2.32}$$

$$\dot{u}_z = \frac{\partial\dot{\phi}_z}{\partial z} + \frac{\partial\dot{\psi}_y}{\partial x} \tag{2.33}$$

The longitudinal wave motion is governed by the equation

$$\nabla^2\phi = \frac{1}{C_L^2}\frac{\partial^2\phi}{\partial t^2} \tag{2.34}$$

while the transverse wave motion is obtained from

$$\nabla^2\bar{\psi} = \frac{1}{c_T^2}\frac{\partial^2\bar{\psi}}{\partial t^2} \tag{2.35}$$

c_L and c_T are given by Equations 2.18 and 2.19 respectively.

There are three basic boundary conditions which must be satisfied at the liquid-solid interface:

(1) The normal compressive stress on the solid and liquid interfaces are equal.

(2) Since the liquid will not support a shear stress, this stress must be zero at the boundary.

(3) The u_z solid and u_z liquid displacement components are equal at the boundary.

Now from the stress-strain relations given by Equations 2.1-2.12

$$\sigma_{zz} = \lambda\left\{\frac{\partial u_x}{\partial x} + \frac{\partial u_z}{\partial z}\right\} + 2G\frac{\partial u_z}{\partial z} \tag{2.36}$$

$$\sigma_{xz} = G\left\{\frac{\partial u_x}{\partial z} + \frac{\partial u_z}{\partial x}\right\} \tag{2.37}$$

Since all quantities are assumed dependent only on x and z then from reference [9]:

$$\bar{\psi}_S = h(x,z)\hat{j} \tag{2.38}$$

Use of Equations 2.37, 2.35 and 2.17 and noting that G=0 for liquid media, boundary condition (1) requires that

$$\lambda_\ell \nabla^2 \phi_\ell = \lambda_S \nabla^2 \phi_S + 2G \left\{ \frac{\partial^2 \phi_S}{\partial z^2} + \frac{\partial^2 \psi_S}{\partial x \, \partial z} \right\} \tag{2.39}$$

and with the time derivative,

$$\lambda_\ell \nabla^2 \dot{\phi}_\ell = \lambda_S \nabla^2 \dot{\phi}_S + 2G \left\{ \frac{\partial^2 \dot{\phi}_S}{\partial z^2} + \frac{\partial^2 \dot{\psi}_S}{\partial x \, \partial z} \right\} \tag{2.40}$$

The shear stress boundary condition requires that

$$2 \frac{\partial^2 \phi_S}{\partial x \, \partial z} + \frac{\partial^2 \psi_S}{\partial x^2} - \frac{\partial^2 \psi_S}{\partial z^2} = 0 \tag{2.41}$$

and with the time derivative,

$$2 \frac{\partial^2 \dot{\phi}_S}{\partial x \, \partial z} + \frac{\partial^2 \dot{\psi}_S}{\partial x^2} - \frac{\partial^2 \dot{\psi}_S}{\partial z^2} = 0 \tag{2.42}$$

The maintenance of continuity at the interface results in the expression:

$$\frac{\partial \phi_\ell}{\partial z} = \frac{\partial \phi_S}{\partial z} + \frac{\partial \psi_S}{\partial x} \tag{2.43}$$

and with the time derivative,

$$\frac{\partial \dot{\phi}_\ell}{\partial z} = \frac{\partial \dot{\phi}_S}{\partial z} + \frac{\partial \dot{\psi}_S}{\partial x} \tag{2.44}$$

From Figure 3 and Equation 2.25 the potential function [9] for the incident wave may be expressed as

$$\dot{\phi}_{inc} = A\exp[i(k_{1\ell}(x \sin\alpha - z \cos\alpha) - wt)] \tag{2.45}$$

and for the reflected wave

$$\dot{\phi}_{refl} = A \frac{A_{rL}}{A_{iL}} \exp[i(k_{1\ell}(x \sin\alpha + z \cos\alpha) - wt)] \tag{2.46}$$

Now for the longitudinal wave in the solid

$$\dot{\phi}_S = A \frac{A_{tL}}{A_{iL}} \exp[i(k_{2\ell}(x \sin\varepsilon - z \cos\varepsilon) - wt)] \tag{2.47}$$

$$\dot{\psi}_S = A \frac{A_{tS}}{A_{iL}} \exp[i(k_{2S}(x \sin\beta - z \cos\beta) - wt)] \tag{2.48}$$

where,

$$k_{1\ell} = \frac{\omega}{C_{1L}} \tag{2.49}$$

$$k_{2\ell} = \frac{\omega}{C_{2L}} \tag{2.50}$$

$$k_{2S} = \frac{\omega}{C_{2S}} \tag{2.51}$$

Brekhovskikh [9] solves Equations 2.45-2.48, 2.40, 2.42 and 2.44 simultaneously to obtain:

$$\frac{A_{rL}}{A_{iL}} = \frac{z_{2\ell}\cos^2 2\beta + z_{2S}\sin^2 2\beta - z_{1\ell}}{z_{2\ell}\cos^2 2\beta + z_{2S}\sin^2 2\beta + z_{1\ell}} \tag{2.52}$$

$$\frac{A_{tL}}{A_{iL}} = \frac{\rho_1}{\rho_2}\frac{2z_{2\ell}\cos 2\beta}{z_{2\ell}\cos^2 2\beta + z_{2S}\sin^2 2\beta + z_{1\ell}} \tag{2.53}$$

$$\frac{A_{tS}}{A_{i\ell}} = \frac{-\rho_1}{\rho_2}\frac{2z_{2S}\sin 2\beta}{z_{2L}\cos^2 2\beta + z_{2S}\sin^2 2\beta + z_{1\ell}} \tag{2.54}$$

where the acoustical impedances are given by,

$$z_{2\ell} = \frac{\rho_2 C_{2L}}{\cos\varepsilon} \tag{2.55}$$

$$z_{2S} = \frac{\rho_2 C_{2S}}{\cos\beta} \tag{2.56}$$

$$z_{1\ell} = \frac{\rho_1 C_{1L}}{\cos\alpha} \tag{2.57}$$

The second case to consider is shown in Figure 4. When a longitudinal wave passes from a solid to liquid medium the following waves result:

(1) a reflected longitudinal wave back into the solid, ArL.

(2) a reflected shear wave back into the solid, ArS.

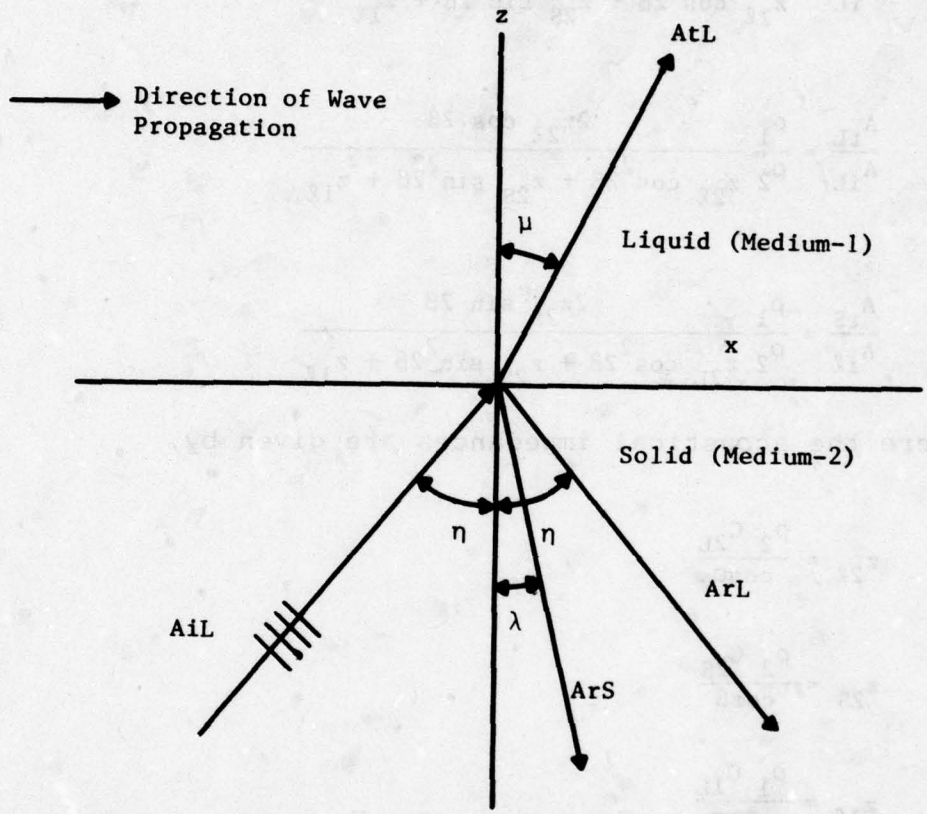

Figure 4. Longitudinal Wave of Amplitude AiL Propagating from Solid to Liquid Media

(3) a transmitted longitudinal wave into the liquid, AtL.

Using the same analysis and boundary conditions as before, Brekhovskikh obtains:

$$\frac{A_{rL}}{A_{iL}} = \frac{z_{1\ell} + z_{2S} \sin^2 2\lambda - z_{2\ell} \cos^2 2\lambda}{z_{1\ell} + z_{2S} \sin^2 2\lambda + z_{2\ell} \cos^2 2\lambda} \tag{2.58}$$

$$\frac{A_{tL}}{A_{iL}} = \left\{\frac{\cos\eta}{\cos\mu \cos^2 2\lambda}\right\} \left\{1 - \frac{A_{rL}}{A_{iL}}\right\} \frac{C_{1L}}{C_{2L}} \tag{2.59}$$

$$\frac{A_{rS}}{A_{iL}} = \left\{\frac{\sin 2\eta}{\cos 2\lambda}\right\} \left\{1 - \frac{A_{rL}}{A_{iL}}\right\} \left\{\frac{C_{2S}}{C_{2L}}\right\}^2 \tag{2.60}$$

where the acoustical impedances are given by:

$$z_{1\ell} = \frac{\rho_1 C_{1L}}{\cos\mu} \tag{2.61}$$

$$z_{2\ell} = \frac{\rho_2 C_{2L}}{\cos\eta} \tag{2.62}$$

$$z_{2S} = \frac{\rho_2 C_{2S}}{\cos\lambda} \tag{2.63}$$

A shear wave passing from a solid to liquid medium and polarized in the xz-plane produces the following waves:

(1) a transmitted longitudinal wave into the liquid medium, AtL.

(2) a reflected shear wave back into the solid, ArS.

(3) a reflected longitudinal wave back into the solid, ArL.

As shown in Figure 5 and using the same analysis as before,

$$\frac{A_{rS}}{A_{iS}} = - \left\{ \frac{z_{1\ell} + z_{2\ell} \cos^2 2\phi - z_{2S} \sin^2 2\phi}{z_{1\ell} + z_{2\ell} \cos^2 2\phi + z_{2S} \sin^2 2\phi} \right\} \tag{2.64}$$

$$\frac{A_{tL}}{A_{iS}} = \left\{ \frac{\tan\psi}{2 \sin^2 \phi} \right\} \left\{ 1 + \frac{A_{rS}}{A_{iS}} \right\} \tag{2.65}$$

$$\frac{A_{rL}}{A_{iS}} = - \frac{\cos 2\phi}{\sin 2\Delta} \left\{ 1 + \frac{A_{rS}}{A_{iS}} \right\} \left\{ \frac{C_{2L}}{C_{2S}} \right\}^2 \tag{2.66}$$

where the acoustical impedances are given by:

$$z_{1\ell} = \frac{\rho_1 C_{1L}}{\cos\psi} \tag{2.67}$$

$$z_{2\ell} = \frac{\rho_2 C_{2L}}{\cos\Delta} \tag{2.68}$$

$$z_{2S} = \frac{\rho_2 C_{2S}}{\cos\phi} \tag{2.69}$$

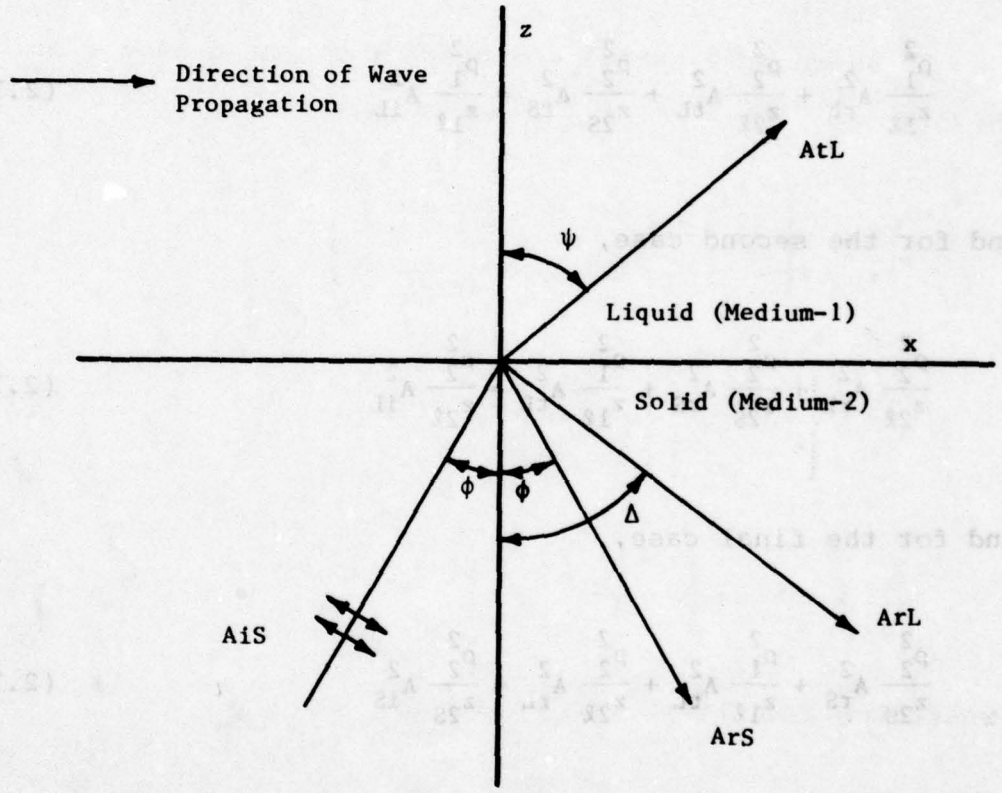

Figure 5. Polarized Shear Wave of Amplitude AiS Propagating from Solid to Liquid Media

Another important parameter in the analysis of wave motion is the conservation of energy at the solid-liquid interface [2]. For the first case, by the conservation of energy:

$$\frac{\rho_1^2}{z_{1\ell}} A_{rL}^2 + \frac{\rho_2^2}{z_{2\ell}} A_{tL}^2 + \frac{\rho_2^2}{z_{2S}} A_{tS}^2 = \frac{\rho_1^2}{z_{1\ell}} A_{iL}^2 \tag{2.70}$$

and for the second case,

$$\frac{\rho_2^2}{z_{2\ell}} A_{rL}^2 + \frac{\rho_2^2}{z_{2S}} A_{rS}^2 + \frac{\rho_1^2}{z_{1\ell}} A_{tL}^2 = \frac{\rho_2^2}{z_{2\ell}} A_{iL}^2 \tag{2.71}$$

and for the final case,

$$\frac{\rho_2^2}{z_{2S}} A_{rS}^2 + \frac{\rho_1^2}{z_{1\ell}} A_{tL}^2 + \frac{\rho_2^2}{z_{2\ell}} A_{rL}^2 = \frac{\rho_2^2}{z_{2S}} A_{iS}^2 \tag{2.72}$$

In general, the energy contained in an acoustical wave may be expressed as [2]:

$$E_{wave} = \frac{\rho_i^2 A_i^2}{z_i} \tag{2.73}$$

where ρ_i, A_i, and Z_i correspond to a shear or longitudinal wave in media i.

Figures 6 and 7 show the division of the energy in an incident longitudinal wave in water as it is transmitted into and reflected from aluminum alloys and plexiglas. These graphs were made using Equations 2.52-2.57 and 2.29. It is interesting to note that very little shear wave energy is generated until the angle of incidence (α) becomes very large. This effect occurs around 9° for transmission from water to aluminum or water to plexiglas. As the angle of incidence increases, the longitudinal transmitted wave energy decreases rapidly while the shear transmitted energy increases to a point and then rapidly decreases. Also it is observed that in general, plexiglas reflects significantly less energy than aluminum and transmits a greater amount of longitudinal wave energy.

In constructing Figures 6 and 7, the following properties of materials were used [1]:

$\rho\ H_2O = 1.0\ g/cm^3$

ρ plexiglas $= 1.20\ g/cm^3$

ρ 17ST-Al $= 2.80\ g/cm^3$

ρ 2SO-Al $= 2.71\ g/cm^3$

$c_{1L}\ H_2O = 1.45 \times 10^5$ cm/sec

c_{2L} plexiglas $= 2.68 \times 10^5$ cm/sec

c_{2L} 17ST-Al $= 6.25 \times 10^5$ cm/sec

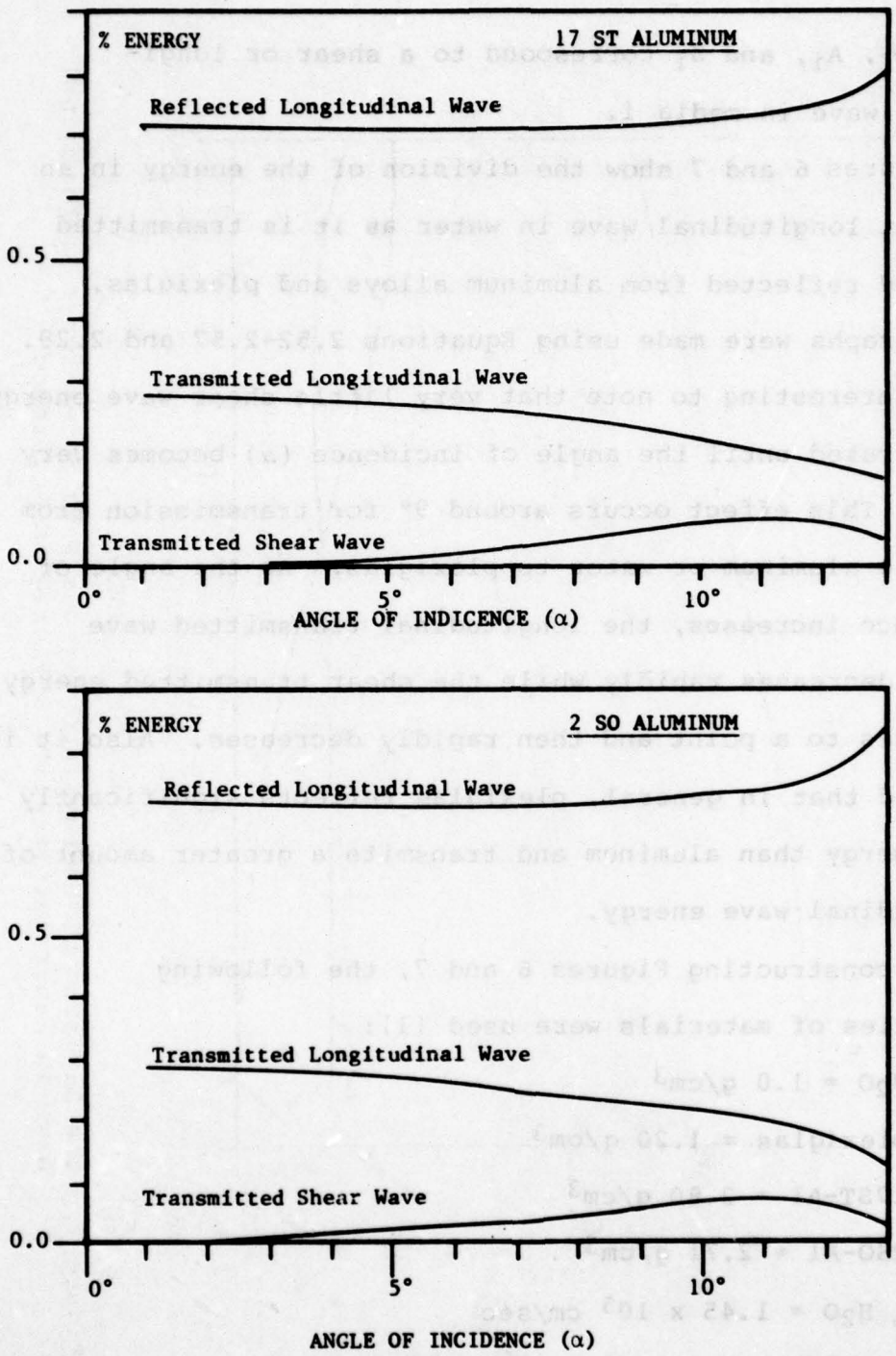

Figure 6. The Division of Energy Into Various Wave Modes for a Longitudinal Wave in Water Intercepting an Aluminum Interface

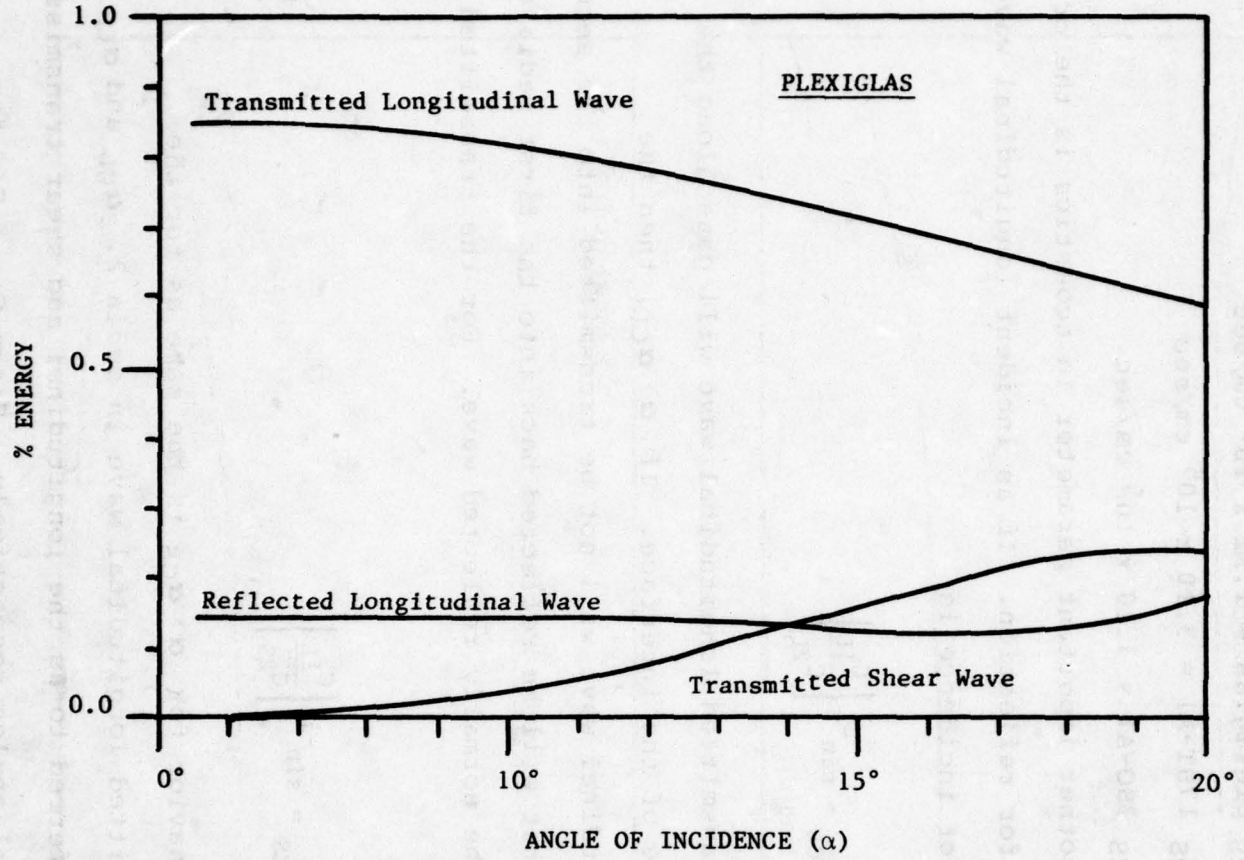

Figure 7. The Division of Energy Into Various Wave Modes for a Longitudinal Wave in Water Intercepting a Plexiglas Interface

c_{2L} 2SO-Al = 6.35×10^5 cm/sec

c_{2S} plexiglas = 1.32×10^5 cm/sec

c_{2S} 17ST-Al = 3.10×10^5 cm/sec

c_{2S} 2SO-Al = 3.10×10^5 cm/sec

Another important parameter in acoustics is the critical angle for reflection. If an incident longitudinal wave angle of incidence is

$$\alpha_{CL} = \sin^{-1}\left\{\frac{C_{1L}}{C_{2L}}\right\} \tag{2.74}$$

the transmitted longitudinal wave will pass along the surface of the interface. If $\alpha > \alpha_{CL}$, then the longitudinal wave will not be transmitted into the second media but will be reflected back into the first media along with the normally reflected wave. For the transmitted shear wave,

$$\alpha_{CS} = \sin^{-1}\left\{\frac{C_{1L}}{C_{2S}}\right\} \tag{2.75}$$

The behavior for $\alpha > \alpha_{CS}$ is the same as for the transmitted longitudinal wave in media 2. α_{CL} and α_{CS} are referred to as the longitudinal and shear transmission critical angles respectively. Since $C_{2L} > C_{2S}$ for solids then $\alpha_{CS} > \alpha_{CL}$. It is possible to use this property for inspecting materials utilizing shear wave

transmission. It is important to note that the analysis developed in this section was for a longitudinal wave in liquid media infinite in width and depth intersecting a solid surface of infinite width and depth. In practice, acoustical waves are very small in lateral dimensions across the wave front. Brekhovskikh [9] shows the existence of small reflected wave displacements in the x-direction for beams of ultrasound having bounded dimensions. This effect is considered negligible in the present analysis.

2.3 Propagation of Sound in an LSL Interface

This section presents the necessary equations for understanding the propagation of sound in an LSL (liquid-solid-liquid) interface. Consider the sound ray diagram of Figure 8. An ultrasonic wave of amplitude A_1 travels along path D_1 until it encounters a liquid-solid interface. At the interface the wave undergoes mode conversion into a shear wave of amplitude A_2, a longitudinal wave of amplitude A_5 and a reflected wave of amplitude A_8. The transmitted shear and longitudinal waves transverse a thickness D of the solid where they encounter a reflecting-scattering layer. This layer is considered to have the unique capability of converting any wave into either a pure shear or longitudinal wave which it reflects back into the solid. There are four possible waves which result:

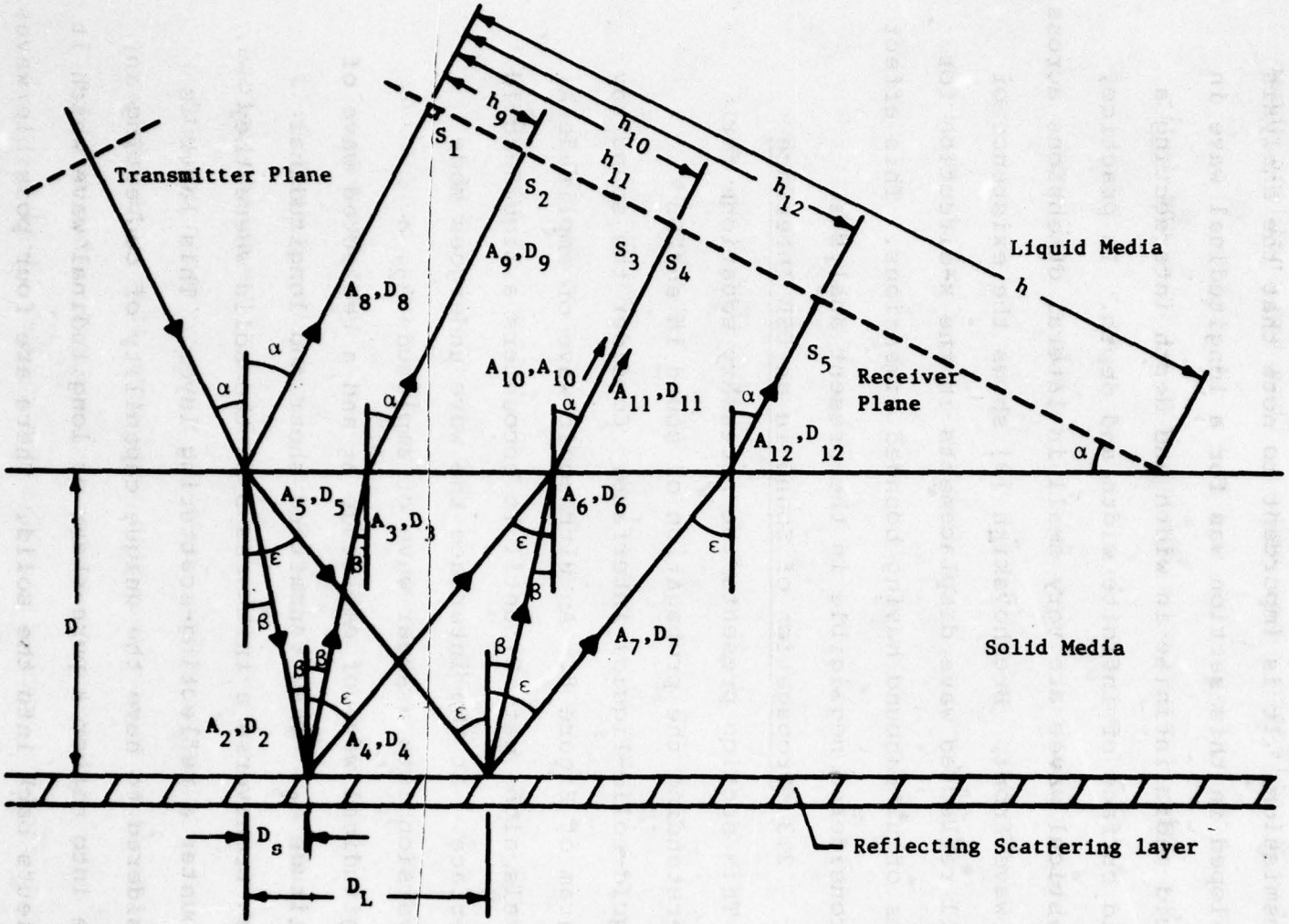

Figure 8. Propagation of Sound in an LSL Interface

(1) a reflected shear wave A_3 from the incident shear wave A_2.

(2) a reflected longitudinal wave A_4 from the incident shear wave A_2.

(3) a reflected shear wave A_6 from the incident longitudinal wave A_5.

(4) a reflected longitudinal wave A_7 from the incident longitudinal wave A_5.

The waves from cases 1,2,3 and 4 undergo further mode conversion at the solid-liquid interface where they are converted into longitudinal waves of amplitudes A_9, A_{10}, A_{11}, and A_{12} respectively. These waves may then be detected as waves of energies S_2, S_3, S_4, and S_5 relative to the transmitted energy, respectivity, in a receiver plane as shown in Figure 8. The waves are assumed to have a Gaussian distribution of intensity versus cross-sectional distance with the maximum occurring along the rays drawn. The effects of bounded beam size are assumed negligible and the basic equations presented in Section 2.2 will be used in the analysis. As stated before, the reflecting-scattering layer is ideal and can convert a longitudinal or shear incident wave with 100% efficiency into either reflected shear or longitudinal waves but not both. Therefore, this layer has one of two ideal

characteristics: it is either a shear reflecting-scattering layer or a longitudinal reflecting-scattering layer.

From the geometry shown in Figure 8 and Snell's law (Equation 2.29)

$$\sin\beta = \frac{C_{2S}}{C_{1L}} \sin\alpha \tag{2.76}$$

$$\sin\varepsilon = \frac{C_{2L}}{C_{1L}} \sin\alpha \tag{2.77}$$

$$D_2 = D_3 = D_6 = \frac{D}{\cos\beta} \tag{2.78}$$

$$D_4 = D_5 = D_7 = \frac{D}{\cos\varepsilon} \tag{2.79}$$

If the following equations are defined:

$$h_9 = 2D_2 \sin\beta \cos\alpha \tag{2.80}$$

$$h_{10} = (D_2 \sin\beta + D_4 \sin\varepsilon) \cos\alpha \tag{2.81}$$

$$h_{11} = (D_5 \sin\varepsilon + D_6 \sin\beta) \cos\alpha \tag{2.82}$$

$$h_{12} = 2D_5 \sin\varepsilon \cos\alpha \tag{2.83}$$

then,

$$h = h_{12} + \frac{D_{12}}{\tan\alpha} \tag{2.84}$$

$$D_{11} = D_{12} \left\{ \frac{h - h_{11}}{h - h_{12}} \right\} \tag{2.85}$$

$$D_{10} = D_{12}\left\{\frac{h - h_{10}}{h - h_{12}}\right\} \tag{2.86}$$

$$D_9 = D_{12}\left\{\frac{h - h_9}{h - h_{12}}\right\} \tag{2.87}$$

$$D_8 = D_{12}\left\{\frac{h}{h - h_{12}}\right\} \tag{2.88}$$

The acoustical impedances for the geometry are:

$$z_{1\ell} = \frac{\rho_1 C_{1L}}{\cos\alpha} \tag{2.89}$$

$$z_{2\ell} = \frac{\rho_2 C_{2L}}{\cos\epsilon} \tag{2.90}$$

$$z_{2S} = \frac{\rho_2 C_{2S}}{\cos\beta} \tag{2.91}$$

In general:

$$S_i \equiv \frac{\text{ENERGY RECEIVED AT LOCATION (i)}}{\text{ENERGY INITIALLY TRANSMITTED}} \tag{2.92}$$

From Equation 2.52 and Equation 2.73

$$S_1^* = \frac{z_{2\ell}\cos^2 2\beta + z_{2S}\sin^2 2\beta - z_{1\ell}}{z_{2\ell}\cos^2 2\beta + z_{2S}\sin^2 2\beta + z_{1\ell}} \tag{2.93}$$

$$S_1 = S_1^* S_1^* \tag{2.94}$$

The calculations for S_2 will be based on a 100% shear reflecting-scattering layer with the shear waves polarized in the xz-plane. Then,

$$\frac{A_3}{A_1} = \frac{-\rho_1}{\rho_2} \frac{2z_{2S} \sin 2\beta}{z_{2\ell} \cos^2 2\beta + z_{2S} \sin^2 2\beta + z_{1\ell}} \tag{2.95}$$

$$\frac{A_9}{A_3} = \left\{ \frac{\tan\alpha}{2\sin^2\beta} \right\} \left\{ 1 + \frac{A_{rS}}{A_{is}} \right\} \tag{2.96}$$

where,

$$\frac{A_{rS}}{A_{is}} = -\left\{ \frac{z_{1\ell} + z_{2\ell} \cos^2 2\beta - z_{2S} \sin^2 2\beta}{z_{1\ell} + z_{2\ell} \cos^2 2\beta + z_{2S} \sin^2 2\beta} \right\} \tag{2.97}$$

and for the energy ratio,

$$S_2^* = \frac{A_3}{A_1} \frac{A_9}{A_3} \tag{2.98}$$

$$S_2 = S_2^* S_2^* \tag{2.99}$$

The S_3 energy ratio is calculated for a 100% longitudinal reflecting-scattering layer. From Equation 2.54,

$$\frac{A_2}{A_1} = -\frac{\rho_1}{\rho_2} \left\{ \frac{2z_{2S} \sin 2\beta}{z_{2\ell} \cos^2 2\beta + z_{2S} \sin^2 2\beta + z_{1\ell}} \right\} \tag{2.100}$$

Equating the conversion of shear wave energy to longitudinal wave energy

$$\frac{\rho_2^2}{z_{2\ell}} A_4^2 = \frac{\rho_2^2}{z_{2S}} A_2^2 \tag{2.101}$$

and,

$$\frac{A_4}{A_1} = \frac{A_2}{A_1}\sqrt{\frac{z_{2\ell}}{z_{2S}}} \tag{2.102}$$

Then from Equation 2.59:

$$\frac{A_{10}}{A_4} = \left\{\frac{\cos\varepsilon}{\cos\alpha\,\cos^2 2\beta}\right\}\left\{1 - \frac{A_{rL}}{A_{iL}}\right\}\frac{C_{1L}}{C_{2L}} \tag{2.103}$$

$$\frac{A_{rL}}{A_{iL}} = \frac{z_{1\ell} + z_{2S}\sin^2 2\beta - z_{2\ell}\cos^2 2\beta}{z_{1\ell} + z_{2S}\sin^2 2\beta + z_{2\ell}\cos^2 2\beta} \tag{2.104}$$

and for the energy ratio,

$$S_3^* = \frac{A_{10}}{A_4}\frac{A_4}{A_1} \tag{2.105}$$

$$S_3 = S_3^* S_3^* \tag{2.106}$$

The S_4 energy ratio may be calculated for a 100% shear reflecting-scattering layer. Using Equation 2.53

$$\frac{A_5}{A_1} = \frac{\rho_1}{\rho_2}\frac{2z_{2\ell}\cos 2\beta}{z_{2\ell}\cos^2 2\beta + z_{2S}\sin^2 2\beta + z_{1\ell}} \tag{2.107}$$

Equating the reflected shear wave energy to the incident longitudinal wave energy

$$\frac{\rho_2^2}{z_{2\ell}}A_5^2 = \frac{\rho_2^2}{z_{2S}}A_6^2 \tag{2.108}$$

$$\frac{A_6}{A_1} = \frac{A_5}{A_1}\sqrt{\frac{z_{2S}}{z_{1\ell}}} \tag{2.109}$$

From Equations 2.64 and 2.65,

$$\frac{A_{11}}{A_6} = \left\{\frac{\tan\alpha}{2\sin^2\beta}\right\}\left\{1 + \frac{A_{rS}}{A_{iS}}\right\} \tag{2.110}$$

$$\frac{A_{rS}}{A_{iS}} = -\left\{\frac{z_{1\ell} + z_{2\ell}\cos^2 2\beta - z_{2S}\sin^2 2\beta}{z_{1\ell} + z_{2\ell}\cos^2 2\beta + z_{2S}\sin^2 2\beta}\right\} \tag{2.111}$$

and for the energy ratio,

$$S_4^* = \frac{A_{11}}{A_6}\frac{A_6}{A_1} \tag{2.112}$$

$$S_4 = S_4^* S_4^* \tag{2.113}$$

Finally, the S_5 energy ratio may be calculated for a 100% longitudinal reflecting-scattering layer. From Equations 2.53, 2.58 and 2.59:

$$\frac{A_7}{A_1} = \frac{\rho_1}{\rho_2}\frac{2z_{2\ell}\cos 2\beta}{z_{2\ell}\cos^2 2\beta + z_{2S}\sin^2 2\beta + z_{1\ell}} \tag{2.114}$$

$$\frac{A_{rL}}{A_{iL}} = \frac{z_{1\ell} + z_{2S}\sin^2 2\beta - z_{2\ell}\cos^2 2\beta}{z_{1\ell} + z_{2S}\sin^2 2\beta + z_{2\ell}\cos^2 2\beta} \tag{2.115}$$

$$\frac{A_{12}}{A_7} = \left\{\frac{\cos\varepsilon}{\cos\alpha\cos^2 2\beta}\right\}\left\{1 - \frac{A_{rL}}{A_{iL}}\right\}\frac{C_{1L}}{C_{2L}} \tag{2.116}$$

and for the energy ratio,

$$S_5^* = \frac{A_{12}}{A_7} \frac{A_7}{A_1}, \tag{2.117}$$

$$S_5 = S_5^* S_5^* \tag{2.118}$$

Figure 9 shows S_1, S_3 and S_5 energy ratios as a function of the angle of incidence (α) for plexiglas where:

$\rho\, H_2O = 1.0\ g/cm^3$

ρ plexiglas $= 1.20\ g/cm^3$

$c_{1L} = 1.448 \times 10^5$ cm/sec

$c_{2L} = 2.68 \times 10^5$ cm/sec

$c_{2S} = 1.32 \times 10^5$ cm/sec

$D_1 = 1.00$ inch

$D_2 = 1.00$ inch

Figure 10 shows h_{12} as a function of the angle of incidence and depth of the scattering layer D. As can be observed in Figure 9, the S_5 ratio is the most dominant ratio for all α given. The S_2 and S_4 ratios were found to be negligible since they involve three rather than two mode conversions from shear to longitudinal and vice versa wave forms. The S_3 ratio is small for it is the result of a longitudinal-shear-longitudinal mode conversion. As illustrated in Figure 7, plexiglas reflects very little incident longitudinal wave energy resulting in a low S_1 ratio.

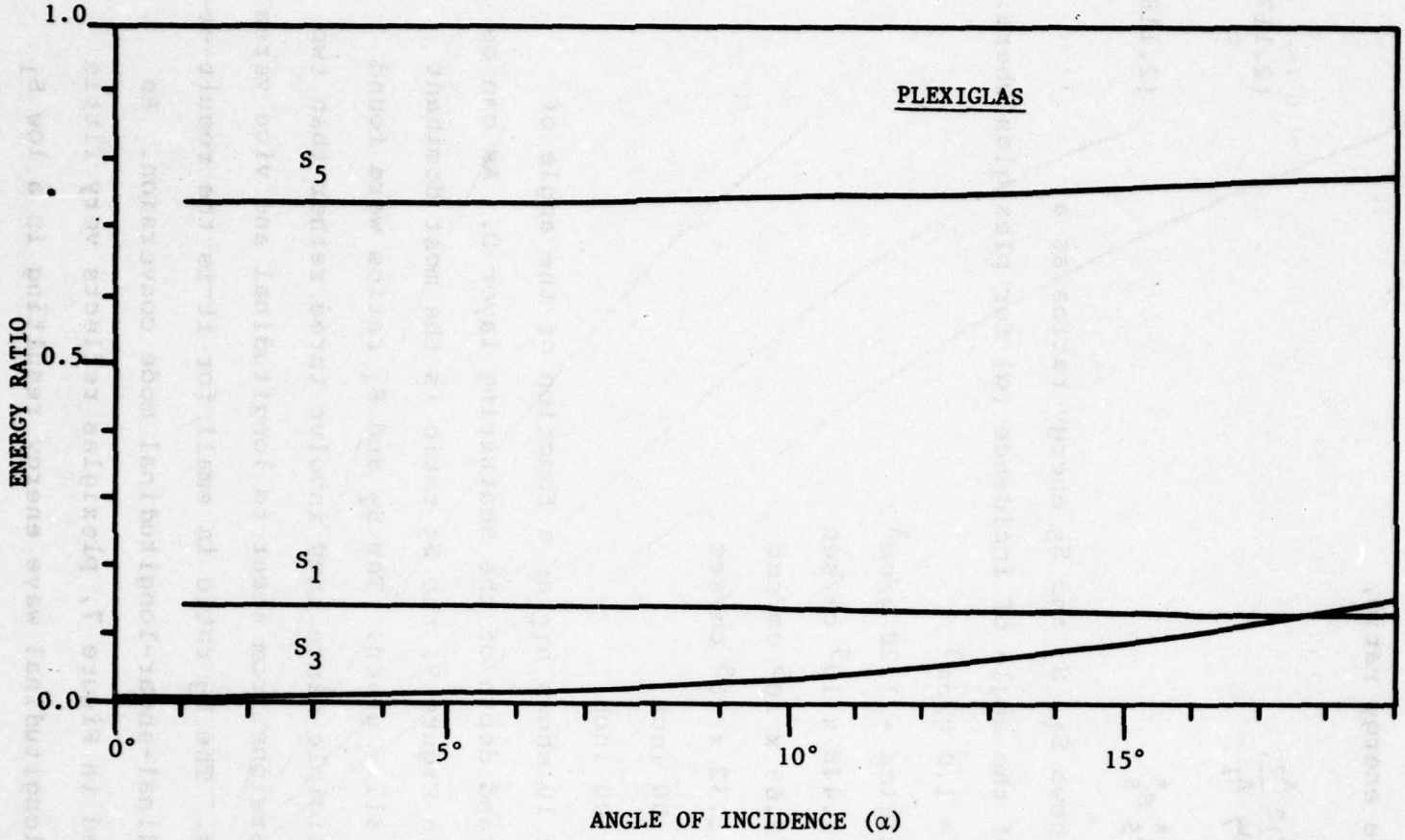

Figure 9. Energy Ratios as a Function of the Angle of Incidence for Transmission of Ultrasound from Water to Plexiglas

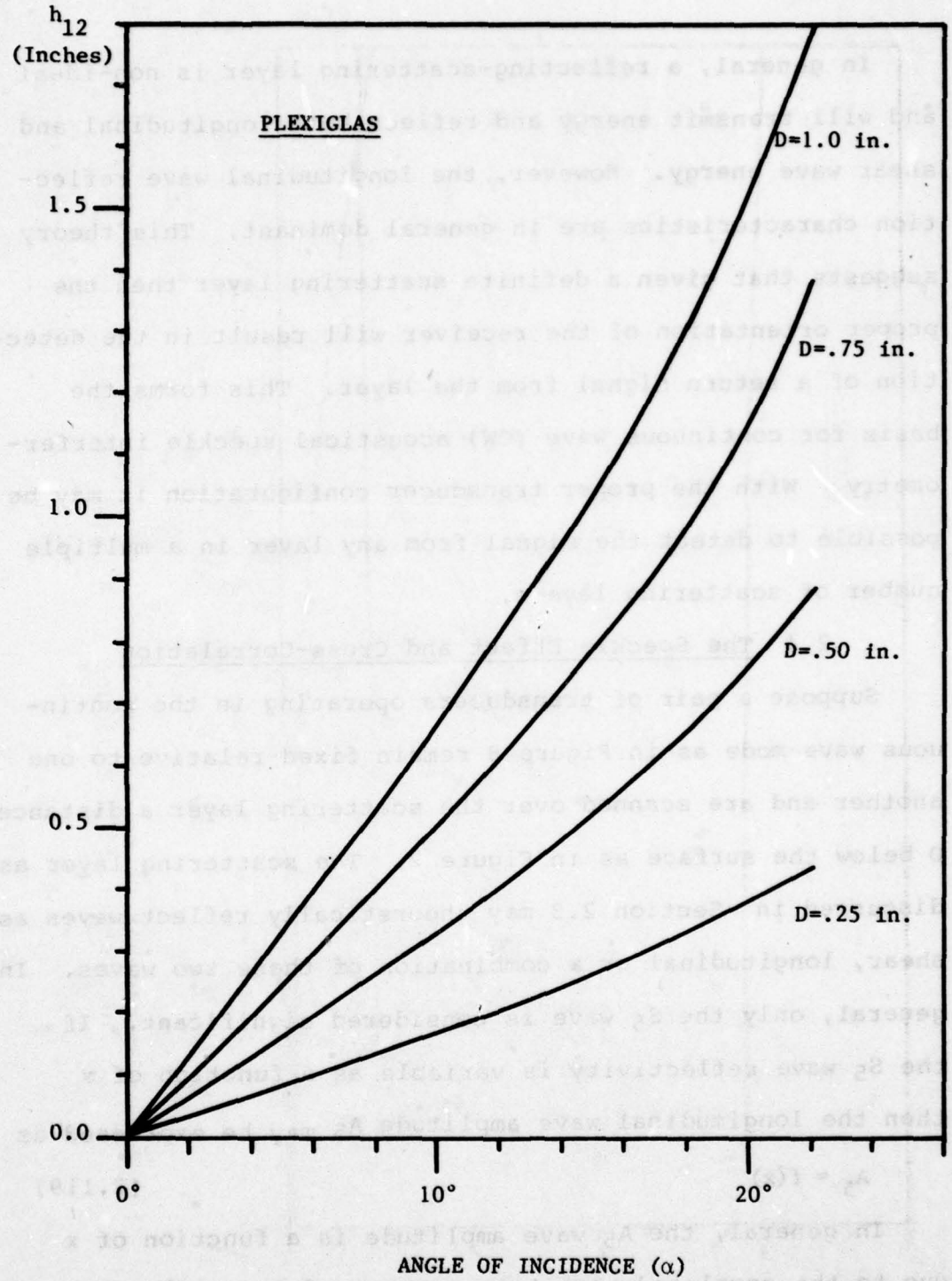

Figure 10. h_{12} Versus Angle of Incidence (α)

In general, a reflecting-scattering layer is non-ideal and will transmit energy and reflect both longitudinal and shear wave energy. However, the longitudinal wave reflection characteristics are in general dominant. This theory suggests that given a definite scattering layer then the proper orientation of the receiver will result in the detection of a return signal from the layer. This forms the basis for continuous wave (CW) acoustical speckle interferometry. With the proper transducer configuration it may be possible to detect the signal from any layer in a multiple number of scattering layers.

2.4 The Speckle Effect and Cross-Correlation

Suppose a pair of transducers operating in the continuous wave mode as in Figure 8 remain fixed relative to one another and are scanned over the scattering layer a distance D below the surface as in Figure 2. The scattering layer as discussed in Section 2.3 may theoretically reflect waves as shear, longitudinal or a combination of these two waves. In general, only the S_5 wave is considered significant. If the S_5 wave reflectivity is variable as a function of x then the longitudinal wave amplitude A_5 may be expressed as

$$A_5 = f(x) \tag{2.119}$$

In general, the A_5 wave amplitude is a function of x due to the completely arbitrary nature of the reflecting-

scattering layer. The random variation in f(x) is referred to as acoustical speckle. Various mechanisms are responsible for the scattering effect. It may be attributed to inclusions in the otherwise assumed homogeneous solid media or in the case of anistropic crystalline structure, grain orientation may produce the effect [1].

Figure 11 shows an example of a continuous wave scan of a reflecting-scattering layer. In the upper portion of the figure, a pair of transducers are oriented for receiving the return echo from the scattering layer which is homogeneous except for a small inclusion. The transducers are scanned from x' to x'+x" and A_5 is plotted as a function of x. Graph (a) shows a decrease in the A_5 amplitude at x=x"' due to the presence of the inclusion. This represents a perturbation in an otherwise straight line plot and may be referred to as acoustical speckle, analogous to a speckle point in laser speckle interferometry.

After scanning the undeformed solid, the transducer pair is returned to its starting position at x=x'. The solid is now displaced an amount Δx and the transducers scan the same scattering layer and the result is shown in graph (b). The process of cross-correlation may be used to determine Δx which is the interferometric analysis process.

Suppose the $A_5(x)$ amplitude is known for the undisplaced solid and the $A_5'(x)$ amplitude variation

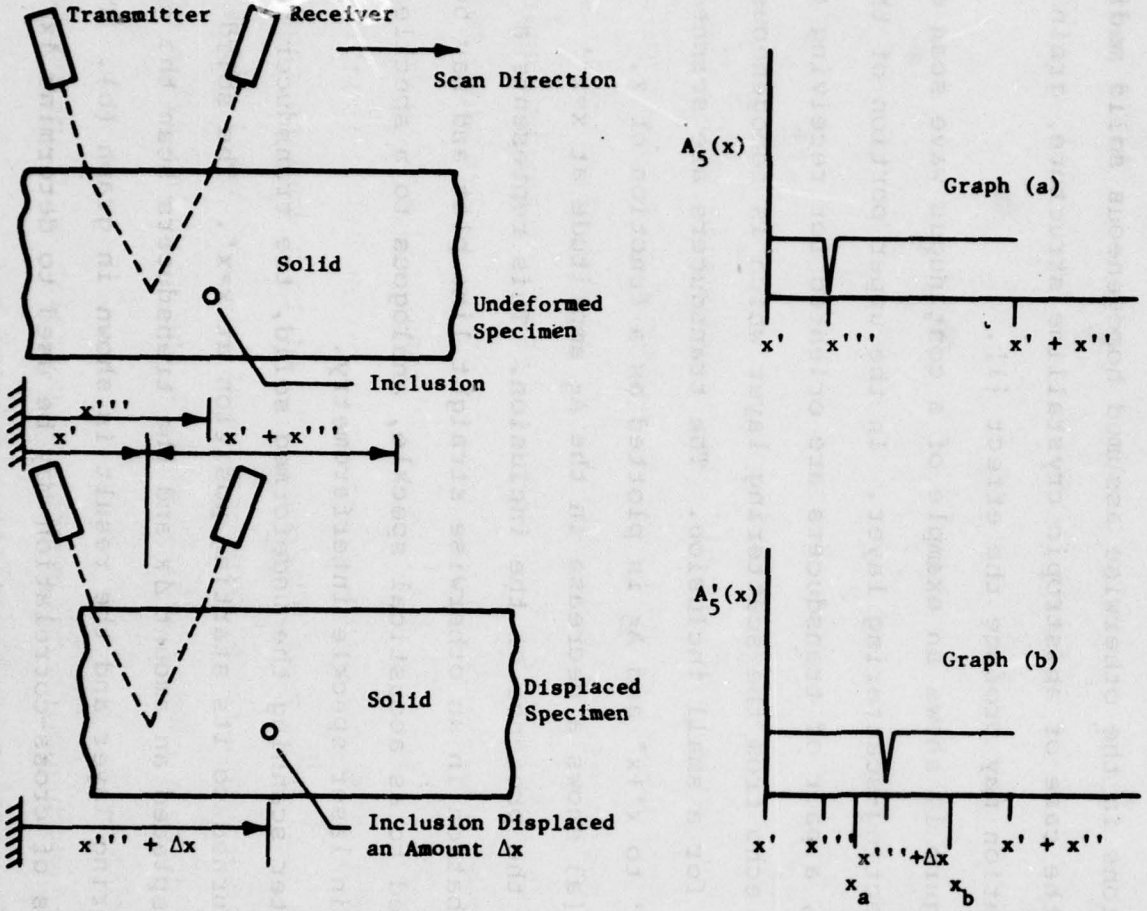

Figure 11. The A_5 Return Echo from an Undeformed and Deformed Solid Scattering Layer

from x_a to x_b is known for the displaced solid. The cross-correlation function [10] is defined as:

$$C(\tau) \equiv \int_{x_a}^{x_b} A_5'(x) A_5(x - \tau) dx \qquad (2.120)$$

where,

$$x_a - x' \leq \tau \leq x_b - x' - x''$$

For the particular example shown, Reference [10] shows that the $C(\tau)$ function will have a maximum for $\tau = \Delta x$. This is the result of the fact that two identical wave forms remain essentially uncorrelated except where they may be superimposed upon each other. The theory indicates that for DC response, $A_5(x)$ signals ($A_5(x)$ = constant) will not result in an extremum. Likewise, for periodic functions $C(\tau)$ will have many extrema. All of this implies that to achieve a desirable cross-correlation, the $A_5(x)$ signal must have a random variation over the scanning range of x' to x'+x".

A much easier to understand correlation function is the difference cross-correlation defined as:

$$C'(\tau) \equiv \int_{x_a}^{x_b} |A_5'(x) - A_5(x - \tau)|dx \qquad (2.121)$$

$$x_a - x' \leq \tau \leq x_b - x' - x''$$

and the least squares cross-correlation function may also be defined as:

$$C''(\tau) \equiv \int_{x_a}^{x_b} [A_5'(x) - A_5(x - \tau)]^2 dx \qquad (2.122)$$

$$x_a - x' \leq \tau \leq x_b - x' - x''$$

Expansion of the least squares cross-correlation function yields:

$$C''(\tau) = \int_{x_a}^{x_b} [A_5'(x)^2 + A_5(x - \tau)^2]dx - 2\,C(\tau) \qquad (2.123)$$

The first term of this equation may be related to the average power of the A_5' and A_5 signals while the last term is the cross-correlation term. Equations 2.121-2.123 have a minima for $\tau = \Delta x$.

It is desirable to utilize Equation 2.122 for correlation for it generally gives the best overall results.

This function weighs both the cross-correlation and the average signal power.

As will be shown in Section III, there are two possible methods for implementing the scanning process. However, both methods use discrete digital sampling of the A_5 and A_5' signals at selected points a distance ΔN apart. Suppose a scan of the undeformed specimen is made from x' to x'+x". A total of N data points were sampled during this scan where $A_5(1) = A_5(x')$ and $A_5(N) = A_5(x'+x")$. The increment between scan points is

$$\Delta N = \frac{x"}{(N - 1)} \tag{2.124}$$

Now let the specimen be displaced a distance

$$\Delta X = -r\Delta N \tag{2.125}$$

The specimen is now scanned $m < N$ times from $x_a = x'$ to x_b where

$$X_b = (M-1)\Delta N \tag{2.126}$$

It is assumed in this analysis that $0 \leq r \leq N-m$ where r is an integer for the present time. The discrete least squares correlation is now

$$C_D"(L) = \sum_{i=1}^{M} [\, A_5'(i) - A_5(i + L) \,]^2 \tag{2.127}$$

$$0 \leq L \leq N - M$$

From the theory presented thus far, the C_D'' function will have a minimum value for L=r. The discrete correlation function

$$C_D(L) = \sum_{i=1}^{M} [\, A_5'(i) A_5(i+L) \,] \qquad (2.128)$$

$$0 \leq L \leq N - M$$

will have a maximum value for L=r.

Equations 2.127 and 2.128 coupled with Equations 2.124 and 2.125 provide the numerical basis for acoustical speckle interferometry. As will be shown later by example, if r is not an integer value for the initial displacement then these equations will interpolate to the nearest integer value. This insures that displacements of $\pm\Delta N$ can be measured. Although the mathematics will not be covered here, it is important to mention that the Discrete Fourier Transform can be used to perform the operation of cross-correlating data involving large N and m values with a considerable time saving in computing if implemented as a Fast Fourier Transform (FFT) algorithm. All correlation analysis presented in this work will be performed using Equation 2.127 as the cross-correlation function.

III. EXPERIMENTAL CONFIGURATION

This section presents the hardware which was used to make acoustical speckle interferograms. Two separate systems are presented. These are the pulse-echo and continuous wave interferometric systems. In developing the two separate systems, eight pieces of hardware comprising the data acquisition system are found common to both.

3.1 Data Acquisition System

Figure 12 illustrates the data acquisition system used in experimentation. The basic components and their functions are:

a.) PDP 11/40 Minicomputer- this computer, manufactured by the Digital Equipment Corporat ı (DEC), serves as the central controller for making an interferogram. It contains 32,000-16 bit words of storage and uses an RT11 software control system.

b.) RX01 Floppy Disk- the disk drive is used to store programs, data and the RT11 monitor. It is a dual drive unit with 250,000-16 bit words of storage. It is manufactured by DEC.

c.) Decwriter- this is the typewriter input/output port for the computer. It is a 30 character per second unit used to input scan parameters for making an

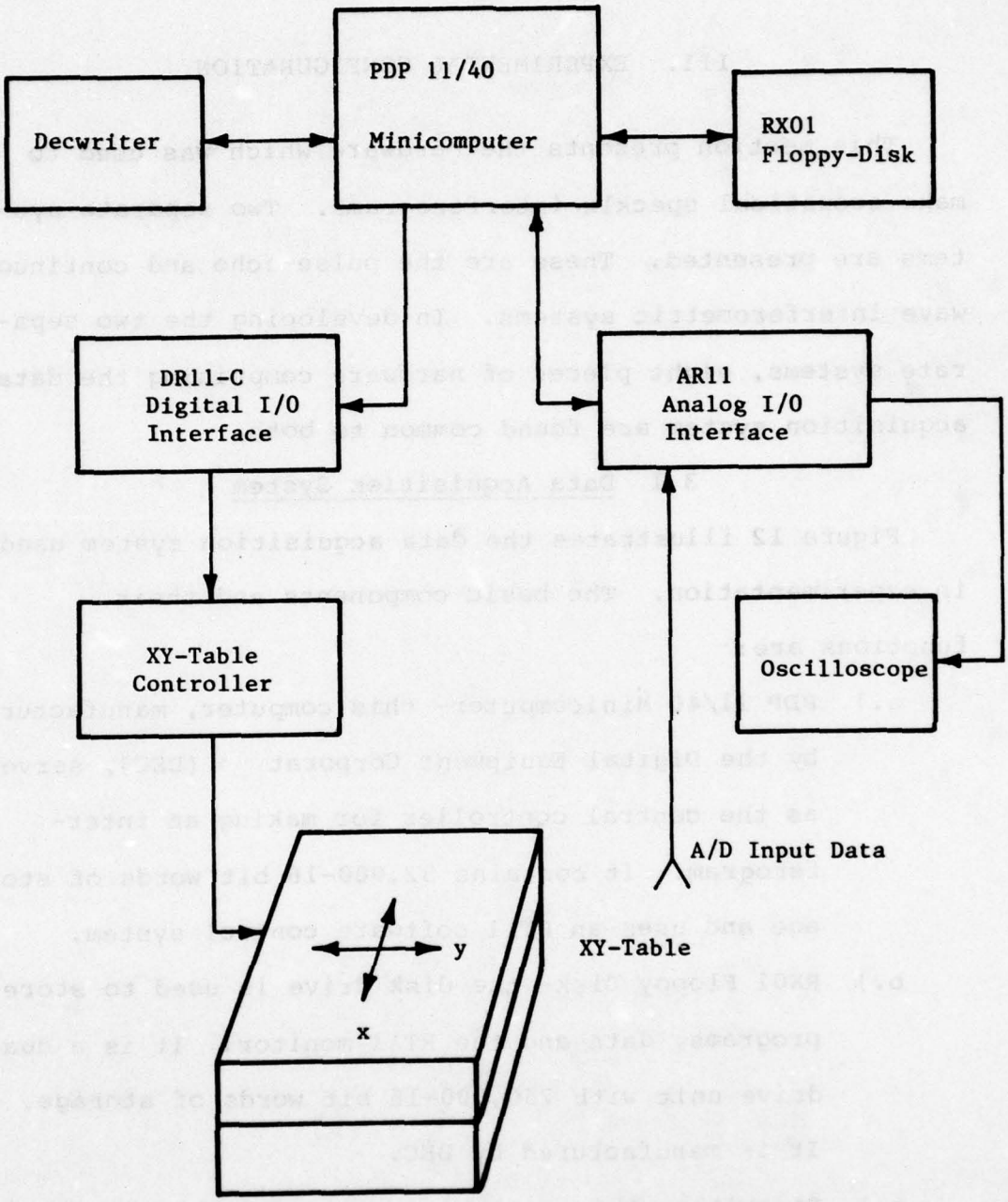

Figure 12. Experimental Apparatus for Data Acquisition

interferogram and printing the results of the correlation process. It is manufactured by DEC.

d.) AR11- this unit is the analog I/O port manufactured by DEC. The AR11 is used to plot data on an oscilloscope and digitalize receiver transducer amplitude signals for the correlation analysis presented in Section 2.4. The AR11 features a 16 channel A/D converter with an input voltage range of 0 to +5 volts, a resolution of 10 bits, and an accuracy of $\pm$0.1% of full scale. It also has a 22 to 24 microsecond conversion time, an input impedance of 10 megohms and a settling time of 8 microseconds maximum. The AR11 also has two D/A converters operating at $\pm$0.5 volts with 10 bits of resolution and $\pm$2% of 1 volt full scale accuracy. These D/A converters are used for plotting data on an oscilloscope.

e.) Oscilloscope- this is a Tektronix Company Model 549 oscilloscope which is used to plot data from the computer via the AR11 interface.

f.) DR11C- the DR11C is a digital I/O interface used to position an XY-table for the transducers when scanning. It is manufactured by DEC and features 16 ports of input and 16 ports of output TTL compatible voltages.

g.) XY-Table Controllers- control of the XY-table via the DR11C interface is maintained by these units. This system contains two Slo-Syn translator modules (Type STM 101) manufactured by the Superior Electric Company. Also included in the system are two Type MPS-1000 power supplies also made by Superior.

h.) XY-Table- the XY-table is one of the most important components in the data acquisition system. It is used to position the transducers for scanning over a specimen in the interferogram process. The XY-table selected is made by Design Components Inc., and is a Model DC-66 having a scanning range of 6 inches in the x and y directions. It can take single steps between scan points of .001 inch with a repositioning accuracy of .0001 inch.

The theory of operation for the data acquisition system is as follows. After the program for scanning is started the necessary scan parameters are input to the computer from the Decwriter. These parameters include the number of points in the first and second scans, the number of .001 inch steps between scan points and the rate at which the scanning process is performed. The computer is then ready for the start of scanning.

For the first scan, the XY-table is advanced to each scan point and a predetermined number of samples of the

receiver transducer output are digitalize and averaged together to obtain the first signal for cross-correlation. After the first scan is made, the specimen is displaced and a second scan is made according to Section 2.4. Cross-correlation of the two signals is then made and the results are printed on the decwriter and plotted on the oscilloscope. Displacement of the specimen is made by moving the transducer(s) relative to the specimen in .001 inch increments.

3.2 Pulse-Echo Experimental Configuration

Pulse-echo acoustical interferometry is similar to sonar scanning. A pulse of 1 to 4 microseconds duration of ultrasound is transmitted from a transducer as shown in Figure 13. The pulse propagates toward the liquid-solid interface where a portion is reflected back to the same transducer which is now acting as a receiver. The energy not reflected back is transmitted into the material. Due to the presence of subsurface inclusions and crystalline grain structure, various parts of the solid may reflect acoustical energy back to the transducer some time after the arrival of the front surface echo.

After the transmitting transducer has been switched to receiver mode the entire echo from the solid-liquid interface and subsurface anomalies is amplified and gated. Figure 14 illustrates the gating process. A square-wave

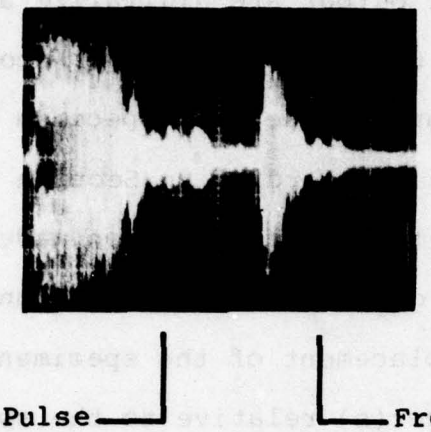

Scale - 0.2 Volt/Division

1 Microsecond/Division Sweep Time

4.08 MHz Transmit Frequency

DAPCO Needle Probe

Figure 13. Pulse Echo Signal of Plexiglas (Specimen-1)

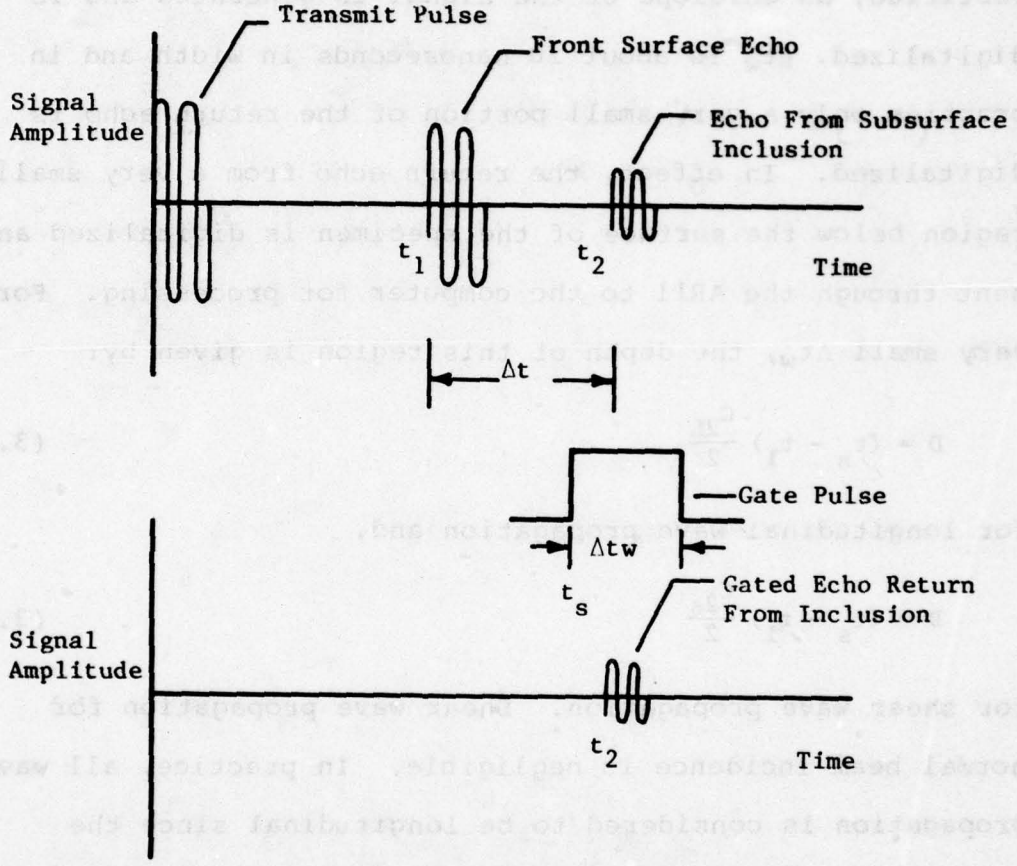

Figure 14. Gating Process for Pulse-Echo Acoustical Speckle Interferometry

pulse of width Δt_w (some time t_s after the initial ultrasound pulse transmission) is activated. When the pulse is turned on the amplified signal of the return echo is rectified, an envelope of the signal is generated and is digitalized. Δt_w is about 20 nanoseconds in width and in practice only a very small portion of the return echo is digitalized. In effect, the return echo from a very small region below the surface of the specimen is digitalized and sent through the AR11 to the computer for processing. For very small Δt_w, the depth of this region is given by:

$$D = (t_s - t_1) \frac{C_{2L}}{2} \tag{3.1}$$

for longitudinal wave propagation and,

$$D = (t_s - t_1) \frac{C_{2s}}{2} \tag{3.2}$$

for shear wave propagation. Shear wave propagation for normal beam incidence is negligible. In practice, all wave propagation is considered to be longitudinal since the transmitting transducer is normal to the solid surface.

Figure 15 illustrates the system used to implement the pulse-echo interferometric process. A Holosonics Company, Model 200 acoustical scanner, capable of transmitting short ultrasonic pulses and converting the echo amplitude to a level representation for any portion of the specimen was used. The unit is commercially available from the

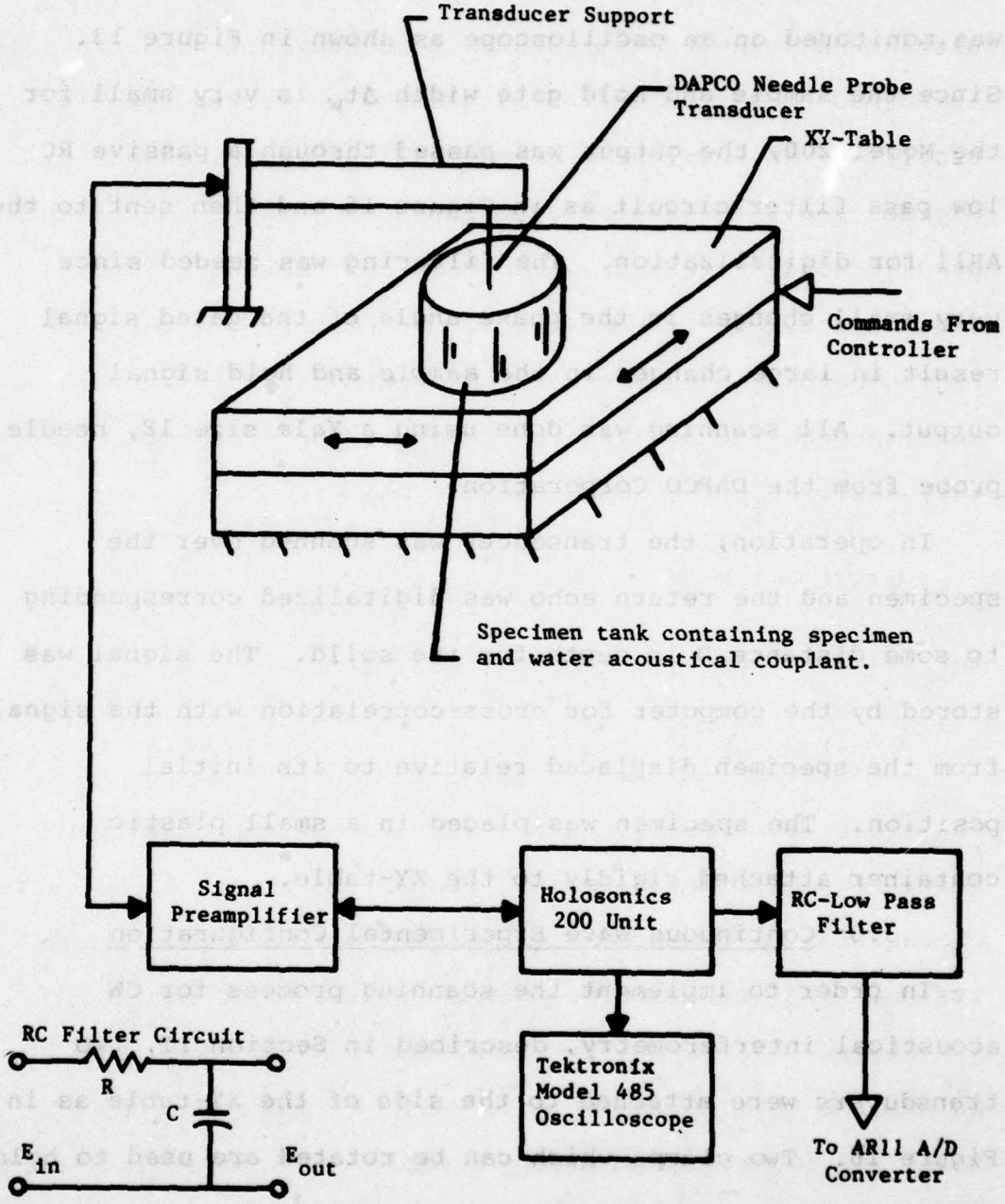

Figure 15. Basic Pulse-Echo Scanning Configuration

Holosonics Corporation. The echo return from the transducer was monitored on an oscilloscope as shown in Figure 13. Since the sample and hold gate width Δt_w is very small for the Model 200, the output was passed through a passive RC low pass filter circuit as in Figure 15 and then sent to the AR11 for digitalization. The filtering was needed since very small changes in the phase angle of the gated signal result in large changes in the sample and hold signal output. All scanning was done using a Yale size 18, needle probe from the DAPCO Corporation.

In operation, the transducer was scanned over the specimen and the return echo was digitalized corresponding to some distance D in depth for the solid. The signal was stored by the computer for cross-correlation with the signal from the specimen displaced relative to its initial position. The specimen was placed in a small plastic container attached rigidly to the XY-table.

3.3 Continuous Wave Experimental Configuration

In order to implement the scanning process for CW acoustical interferometry, described in Section II, two transducers were attached to the side of the XY-table as in Figure 16. Two clamps which can be rotated are used to hold the transducers in their proper orientation for scanning. These transducers were immersed in a tank of water containing the specimen and scanned over its surface.

(a)

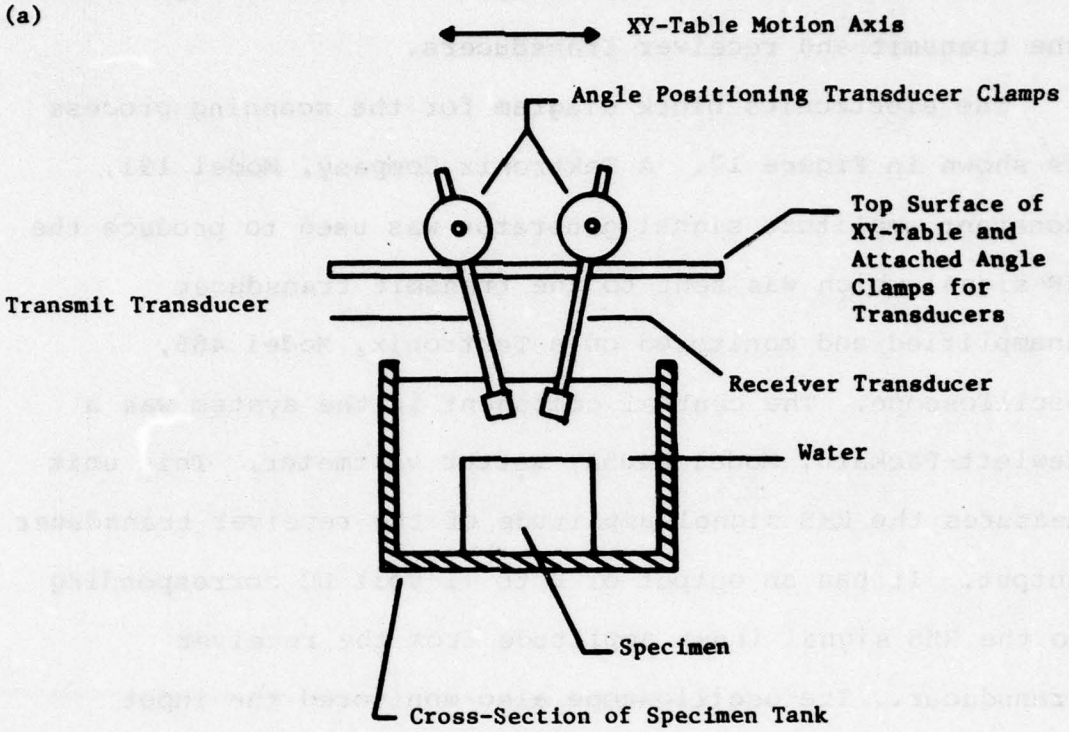

(b)

Upper Trace = 2 V/Div
Lower Trace = .2 V/Div
3.08 MHz Signal

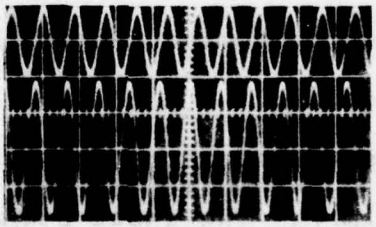

Figure 16. (a) Basic Continuous Wave Scanning Geometry
(b) Transmit and Receiver CW Signals

Figure 16 illustrates a set of typical 3.08 MHz signals from the transmit and receiver transducers.

The electronics block diagram for the scanning process is shown in Figure 17. A Tektronix Company, Model 191, constant amplitude signal generator was used to produce the RF signal which was sent to the transmit transducer unamplified and monitored on a Tektronix, Model 485, oscilloscope. The central component in the system was a Hewlett-Packard, Model 8405A, vector voltmeter. This unit measures the RMS signal amplitude of the receiver transducer output. It has an output of 0 to +1 volt DC corresponding to the RMS signal input amplitude from the receiver transducer. The oscilloscope also monitored the input voltage to the vector voltmeter. The Model 8405A provides a stable output signal corresponding to the input signal. Its output was sent directly to the AR11 without any need for electronic filtering.

In practice, the transducers were scanned over the surface of the specimen. The input signal to the transmit transducer remained fixed while the receiver transducer signal was monitored by the 8405A and digitalized by the AR11. After the first scan was made, the transducers were displaced relative to the specimen and the second scan was made. The signals were then cross-correlated to determine the displacement between scans.

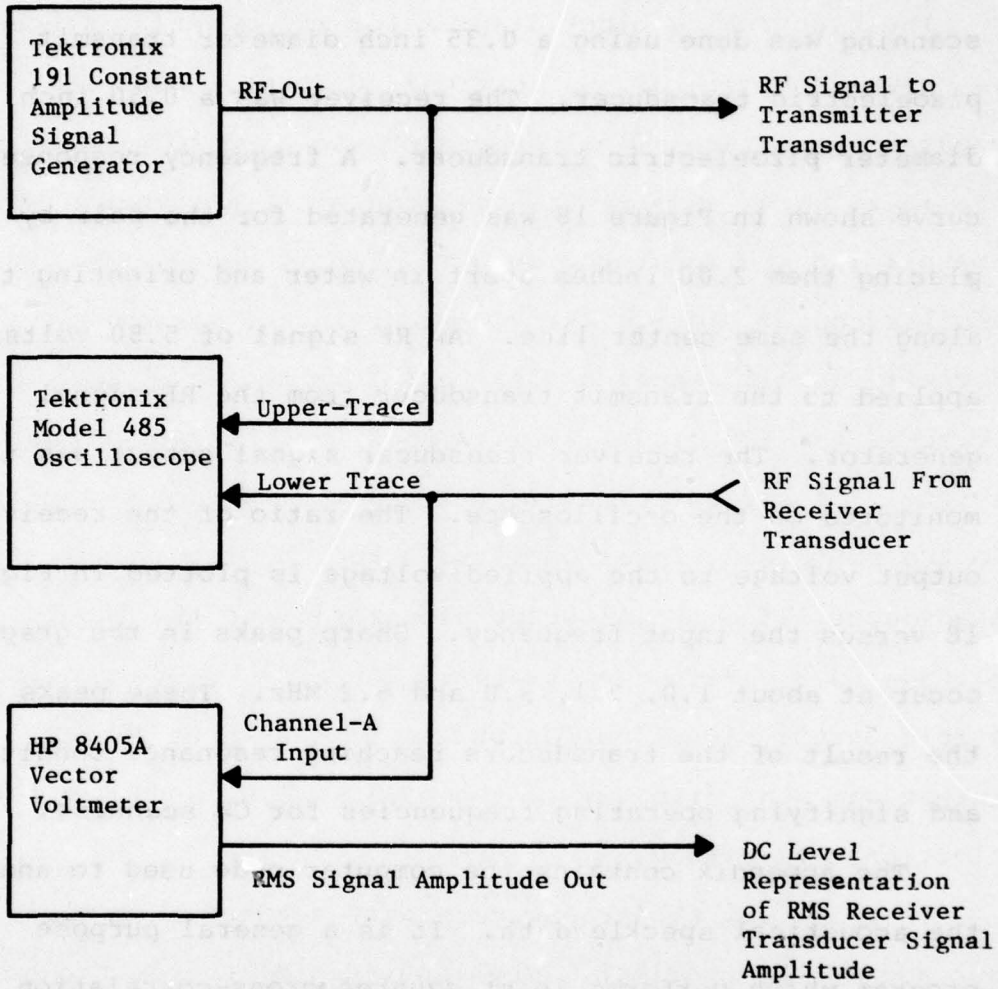

Figure 17. Continuous Wave Scanning Electronics Block Diagram

An important piece of information for CW scanning is the frequency response curve for the transducer pair. All CW scanning was done using a 0.35 inch diameter transmit pizoelectric transducer. The receiver was a 0.50 inch diameter pizoelectric transducer. A frequency response curve shown in Figure 18 was generated for the pair by placing them 2.00 inches apart in water and orienting them along the same center line. An RF signal of 5.80 volts was applied to the transmit transducer from the RF signal generator. The receiver transducer signal output was then monitored on the oscilloscope. The ratio of the receiver output voltage to the applied voltage is plotted in Figure 18 versus the input frequency. Sharp peaks in the graph occur at about 1.0, 2.1, 3.0 and 5.2 MHz. These peaks are the result of the transducers reaching resonance conditions and signifying operating frequencies for CW scanning.

The appendix contains the computer code used to analyze the acoustical speckle data. It is a general purpose program which performs least squares cross-correlation analysis of either CW or pulse-echo signal data.

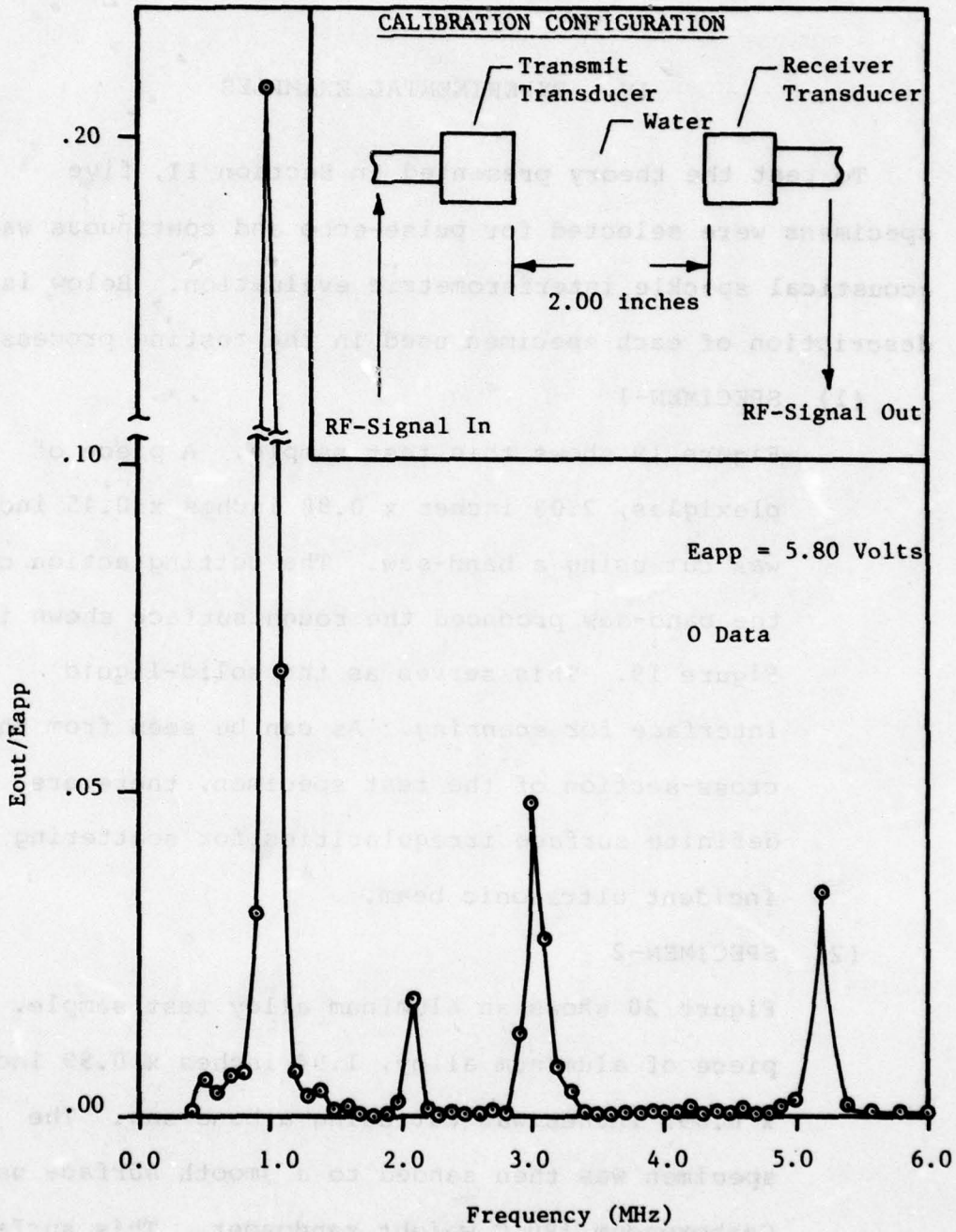

Figure 18. Continuous Wave Scanning Transducer Pair Frequency Response

IV. EXPERIMENTAL EXAMPLES

To test the theory presented in Section II, five specimens were selected for pulse-echo and continuous wave acoustical speckle interferometric evaluation. Below is a description of each specimen used in the testing process:

(1) SPECIMEN-1

Figure 19 shows this test sample. A piece of plexiglas, 2.03 inches x 0.88 inches x 0.45 inches was cut using a band-saw. The cutting action of the band-saw produced the rough surface shown in Figure 19. This serves as the solid-liquid interface for scanning. As can be seen from the cross-section of the test specimen, there are definite surface irregularities for scattering the incident ultrasonic beam.

(2) SPECIMEN-2

Figure 20 shows an aluminum alloy test sample. A piece of aluminum alloy, 1.94 inches x 0.99 inches x 0.095 inches was cut using a band-saw. The specimen was then sanded to a smooth surface using Carborundum 180 C weight sandpaper. This surface is shown in Figure 20-(a). The cross-sectional surface irregularities are very small.

(a)

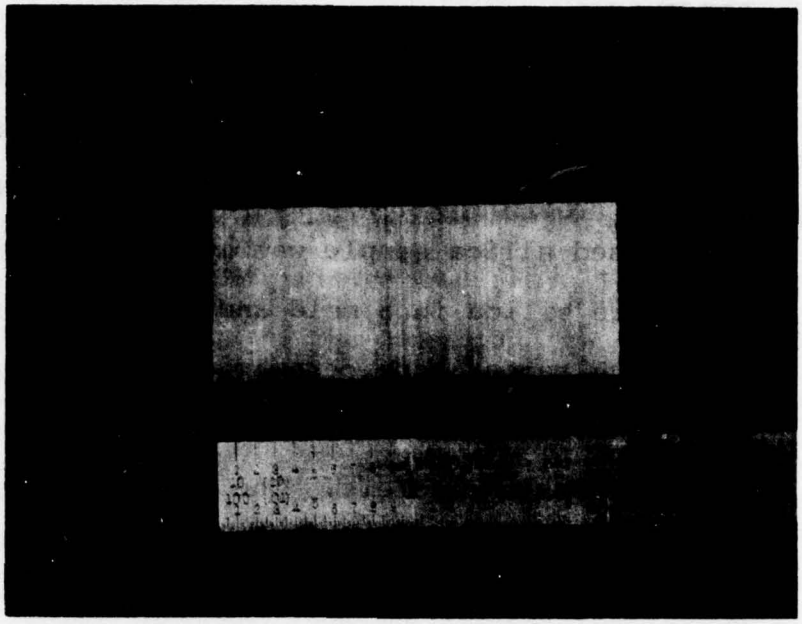

(b)

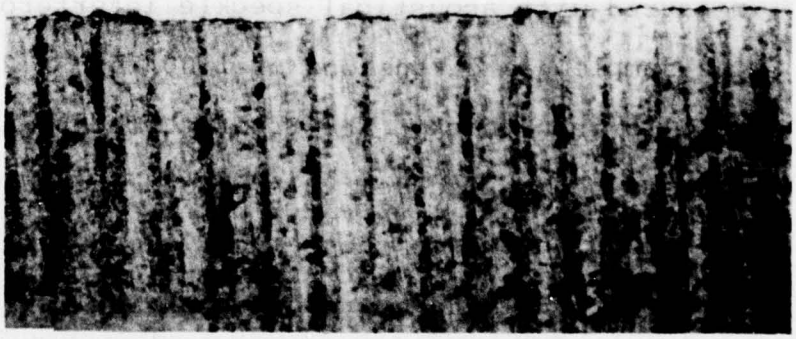

0.0224 inch thick slice of Specimen-1
at 10X magnification

Figure 19. (a) Test Specimen-1 (Plexiglas)
(b) Cross-Section of Specimen-1

(3) SPECIMEN-3

Figure 20-(b) shows a specimen made of slip-cast fused silica. The dimensions of the specimen are 2.00 inch diameter x 0.49 inches thick. The slip-cast fused silica sample was made by compressing very pure silica in a mold and fusing the material in a high temperature ceramic oven. This material is often used for protecting sensitive radar antenna transmission systems. The surface is very smooth and relatively free of internal defects such as small gas bubbles.

(4) SPECIMEN-4

Figure 21-(a) shows a plexiglas specimen fabricated to show that deformation in a material could be measured with acoustical speckle interferometry. The sample has dimensions of 1.00 inch x 2.36 inch x 0.130 inch thick. The front surface, which is exposed to the incident ultrasound and serving as the solid interface, has a very glossy appearance. As such, it gives very poor acoustical speckle information in CW scnning. The back surface, which is shown in Figure 21-(a), was made by cutting grooves 0.04 inches wide and approximately 0.02 inches deep into the plexiglas using a band-saw. The surface was then sanded lightly with Car-

(a)

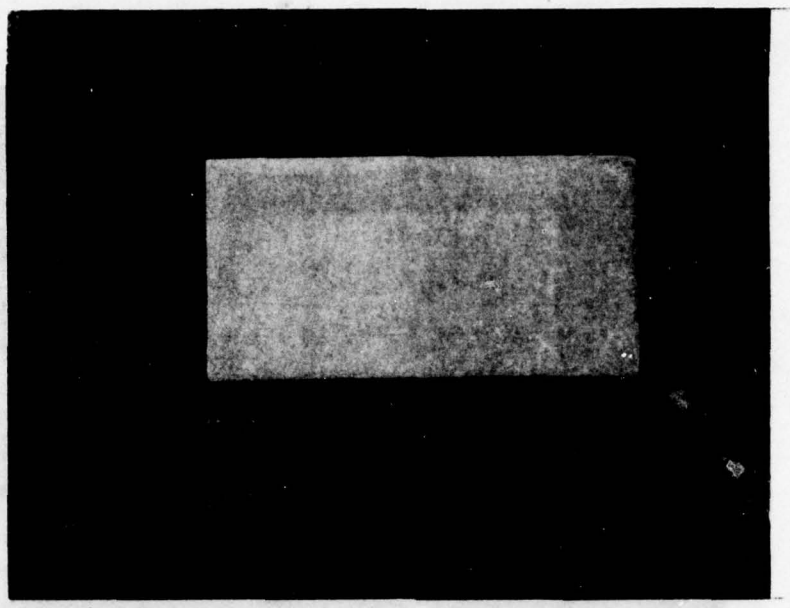

(b)

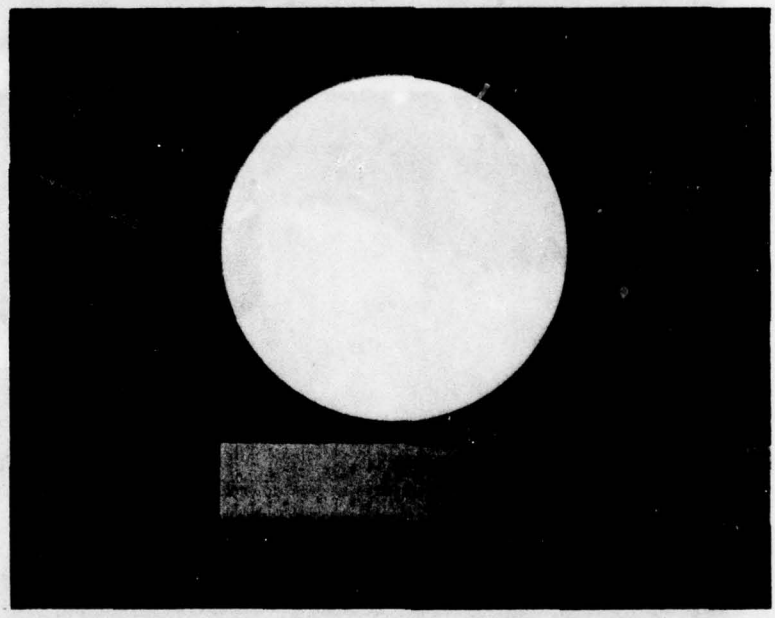

Figure 20. (a) Test Specimen-2 (Aluminum)
(b) Test Specimen-3 (Slip-Cast Fused Silica)

(a)

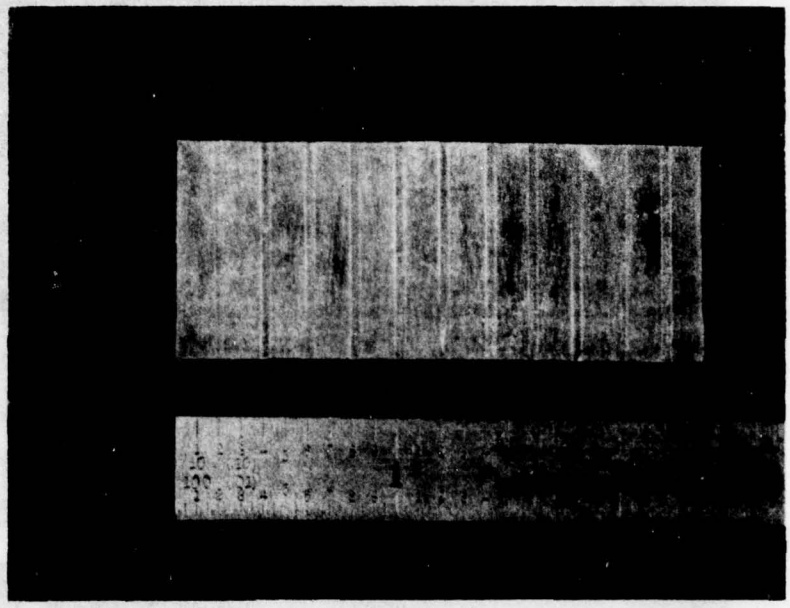

(b)

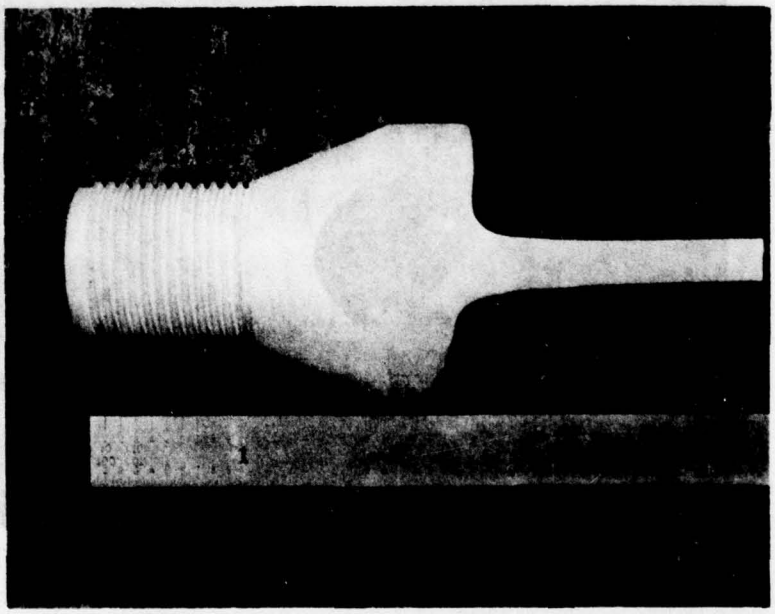

Figure 21. (a) Test Specimen-4 (Plexiglas)
(b) Test Specimen-5 (Aluminum Casting)

borundum 180 C weight sandpaper. This back surface served as a scattering-reflecting layer for acoustical interferometric CW scanning. The grooves were spaced 0.20 inches apart.

(5) SPECIMEN-5

This specimen is shown in Figure 21-(b). The sample is an aluminum casting pitted with gas holes measuring up to 0.13 inches in diameter. The specimen is approximately 0.67 inches thick and has a surface roughness similar to a ground finish obtained from an aluminum sanding wheel. This sample was used to show how pulse-echo scanning could be used to predict internal deformation in solids.

Table-1 gives the property data concerning density and propagation velocities of ultrasound for specimens 1-5. These values are only good approximations since the exact chemical composition of the specimen were unknown.

4.1 Experimental Test-1

In this test, specimen-1 was scanned as shown in Figure 22 a distance of 0.100 inch with 0.001 inch increments for the initial scan. The specimen was then displaced a distance Δx by moving the DAPCO needle probe and then a second scan of 0.050 inches in 0.001 inch increments was made. The two scans were least squares cross-correlated and Δx was predicted based upon the minima in the correlation

TABLE-1

SPECIMEN 1-5 PROPERTY DATA

SPECIMEN	MATERIAL	ρ'	c_{2L}^2	c_{2S}^2
1	Plexiglas	1.20	2.68	1.32
2	Aluminum	2.80	6.25	3.10
3	Slip-Cast Silica	1.96	4.08	2.50
4	Plexiglas	1.20	2.68	1.32
5	Aluminum	2.80	6.25	3.10

Note 1 Density given in g/cm^3

Note 2 Velocity x 10^5 cm/sec

(a) Geometry for Test Scan

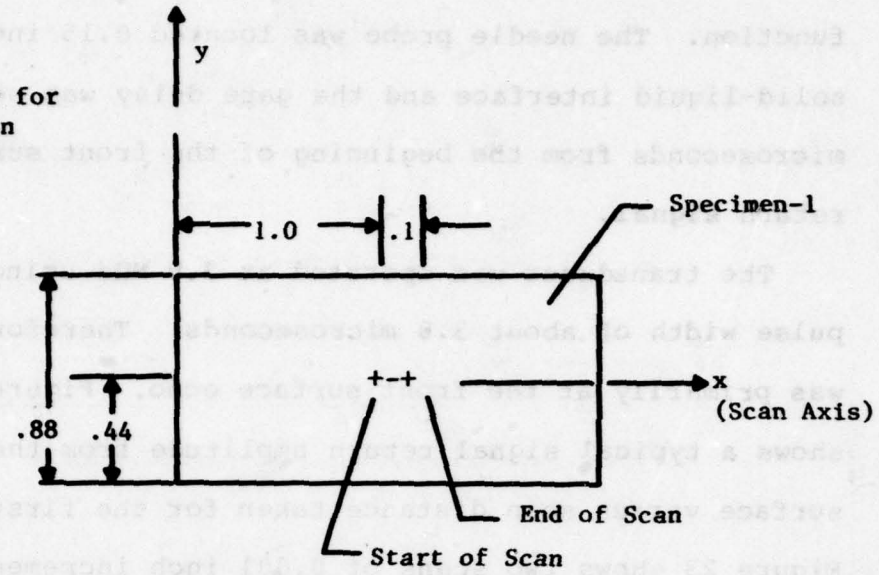

(All dimensions are in inches)

(b) Typical Signal Digitalized by the Computer From the Front-Surface Echo Return for Correlation

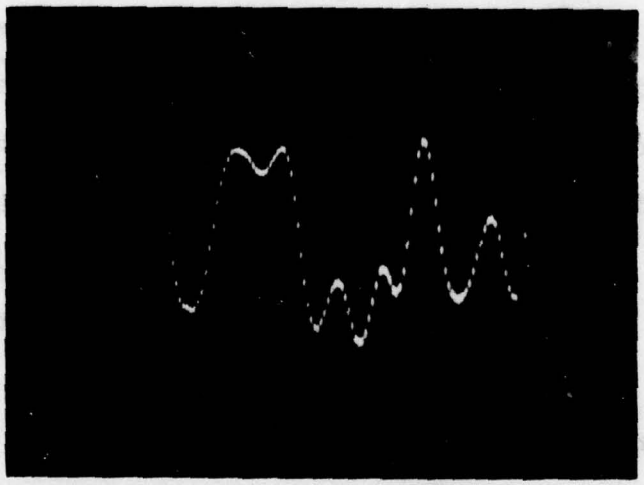

Figure 22. Experimental Test-1 Configuration

function. The needle probe was located 0.15 inch from the solid-liquid interface and the gate delay was set at 0.2 microseconds from the beginning of the front surface echo return signal.

The transducer was operated at 3.9 MHz using a transmit pulse width of about 3.0 microseconds. Therefore, gating was primarily at the front surface echo. Figure 22 also shows a typical signal return amplitude from the front surface versus scan distance taken for the first scan. Figure 23 shows two scans of 0.001 inch increment between A/D samples and a scan axis length of 0.100 inch in which the specimen was displaced 0.001 inch between scans. A phase shift of 0.001 inch between the two scans may be noted.

Figure 24 shows the final result of the test. As illustrated, the correlation technique accurately predicted the displacement of the specimen relative to the transducer for every Δx selected. It is important to note that an average of 1000 samples of the Holosonics Model 200 output were taken for each data point used in correlation to reduce noise.

An average of 30 to 60 seconds is required for obtaining a single data point shown in Figure 24. Therefore, displacement measurements can be made very quickly using the technique. The RC filter used for signal smoothing

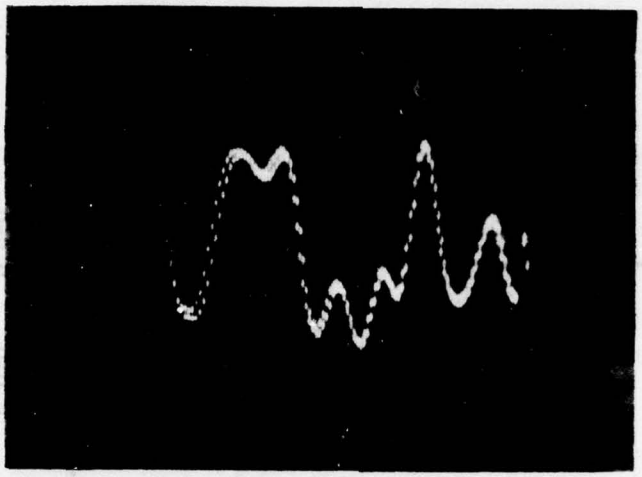

Experimental Test-1 Data: Scan Axis Length = 0.100 Inch

Scan Axis Increment = 0.001 Inch

Sample is Displaced 0.001 Inch Between Scans

Figure 23. First and Second Scans of Specimen-1

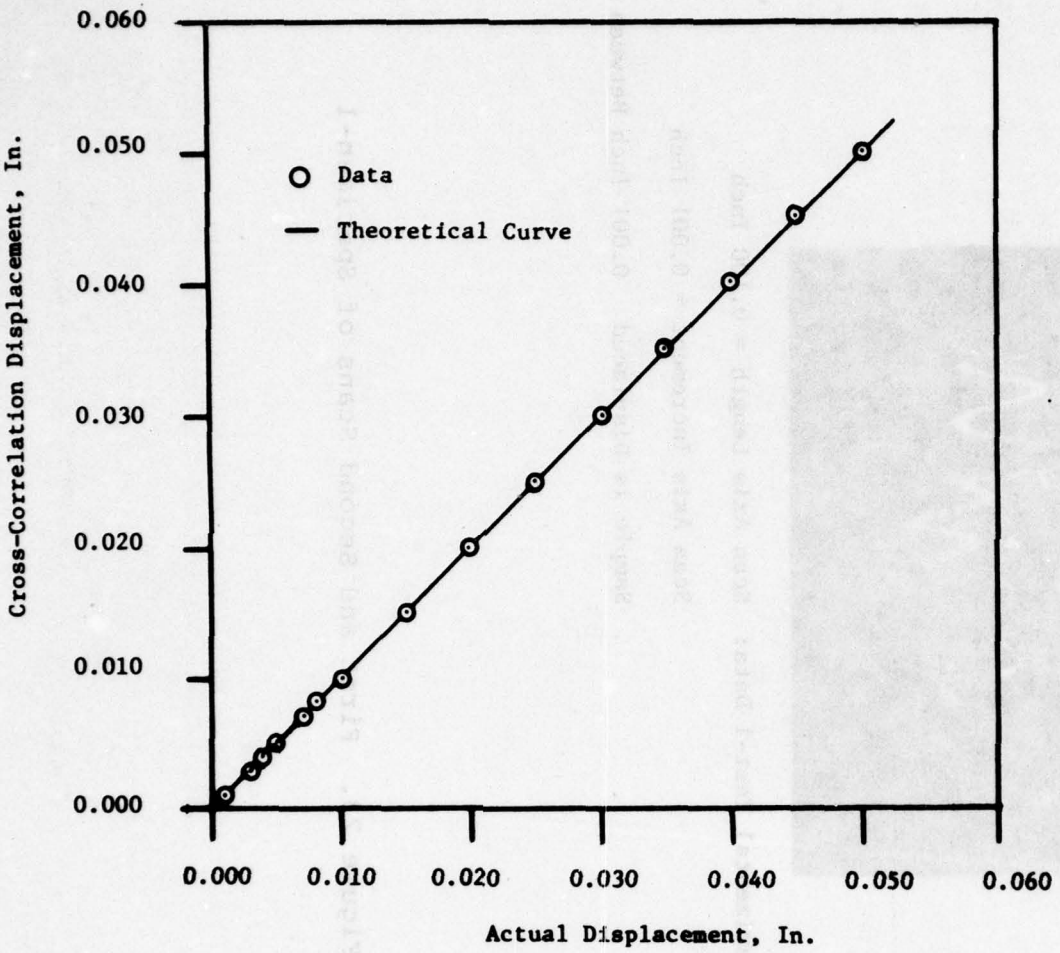

Figure 24. Test-1 Displacement Measured by Cross-Correlation Versus Actual Displacement

described in Section III was a 5.0 KΩ - 25.25 MFD resistor-capacitor combination.

4.2 Experimental Test-2

The process of discrete cross-correlation described in Section II suffers from the distinct disadvantage that the minimum measurable displacement is equal to the scan increment of the XY-table. In this test, the scan parameters are the same as in Test-1 except that the scan increment is 0.002 inch between discrete points. Therefore, the scan axis length for the first scan is 0.200 inch and 0.100 inch for the second. All other sample dimensions and average number of samples per point are the same as in Test-1. The purpose of this test is to examine how well the correlation process can measure displacements when the actual Δx displacement is not an integer multiple of the incremental scan distance between sample points.

Figure 25 shows the results of the test. As can be seen from the figure, when the actual displacement is an integer multiple of the scan increment, the cross-correlation predicted displacement is exactly correct. However, if the actual displacement is between the integer multiples of the scan increment, the predicted displacement is rounded off to the nearest integer multiple.

From these results it is shown that the cross-correlation process can measure actual displacements to the

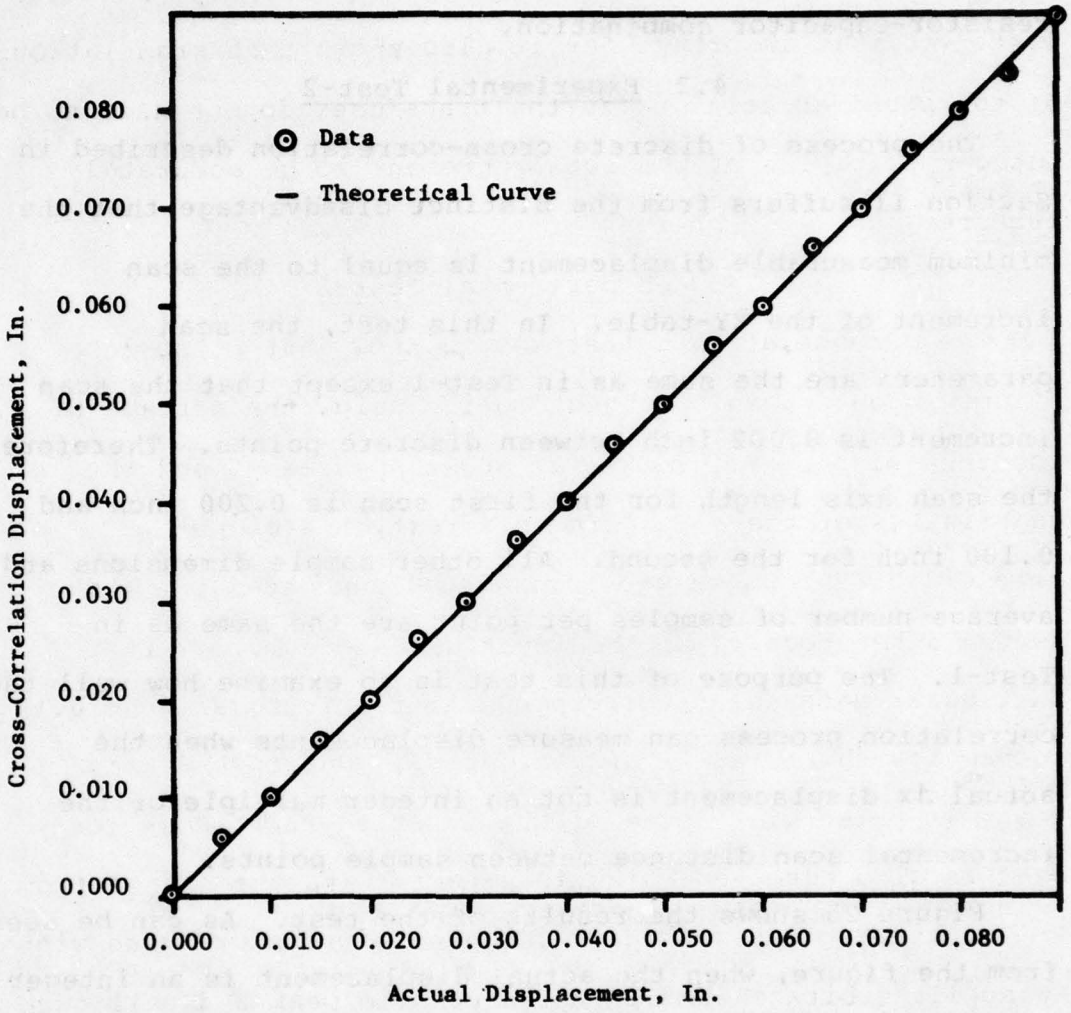

Figure 25. Test-2 Displacement Measured by Cross-Correlation Versus Actual Displacement

nearest value of the scan increment or $\pm$0.002 inch in this test. This is important for it also shows that translations of the specimen relative to the transducer do not have to be integer multiples of the scan increment to be accurately measured.

4.3 Experimental Test-3

The purpose of this test was to show that pulse-echo scanning could resolve object motion below the surface of the test piece. Figure 26-(a) shows Specimen-5 and the coordinates of the scan. In this test, a 4 micro-second-4.05 MHz pulse was transmitted and gated 1 micro-second after receipt of the front surface echo. This particular gate delay corresponds to receiving an echo 0.125 inch below the solid-liquid interface. Due to the long transmit pulse width some of the front surface acoustical echo is also received which interferes with the signal from the scattering layer. The DAPCO needle probe was used with an applied voltage of 1.28 volts peak to peak and 0.11 inch from the solid-liquid interface.

The scan increment for the test was 0.001 inch. The first scan axis length was 0.100 inch and the second axis length was 0.050 inch. Figure 26-(b) shows the digitalized return echo from the scattering layer for the first scan. Each discrete point used in cross-correlation was the result of signal averaging the return echo over 1000 samples.

(a)

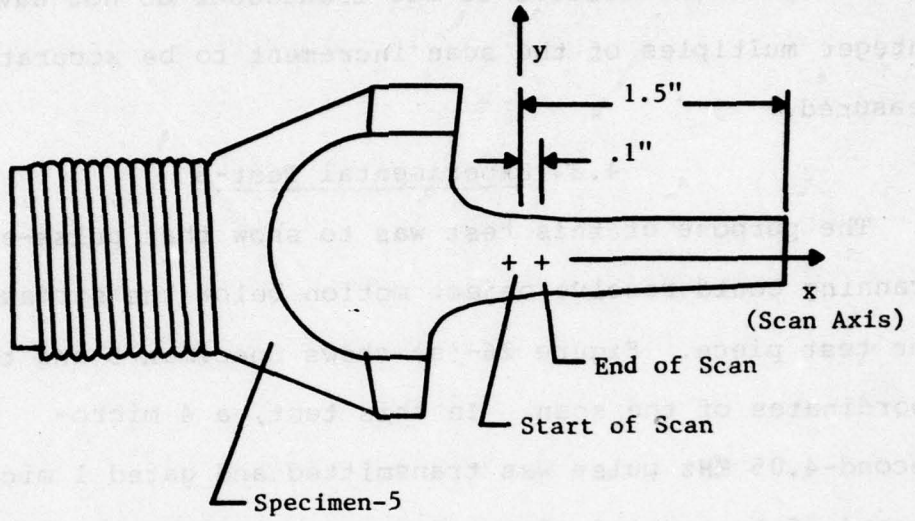

(b)

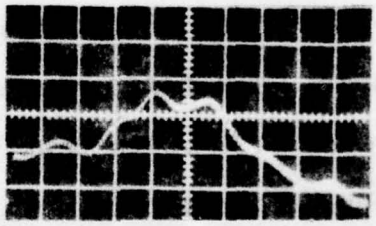

Figure 26. Test-3 Experimental Scan
(a) Scan Geometry Showing Specimen
(b) First Scan Used in Cross-Correlation

Figure 27 shows the results of the test. As can be seen, there is a great deal of scatter in the data. This is due to the fact that the return echo from the acoustical scattering layer is very low in amplitude. The low amplitude signal is a result of the poor transmissivity of ultrasound from water to aluminum (Figure 6). Since the return echo has to be amplified a great deal which introduces spurious noise, a poor signal for correlation is the ultimate result. The overall results are still favorable despite this problem.

4.4 Experimental Test-4

The purpose of this test was to verify that CW acoustical interferometry could predict motion displacement of specimen based upon the theory presented in Section II. Figure 28-(a) shows the basic experimental geometry for the test. As can be seen from the scaled figure, the receiver detects energy below the surface of Specimen-2 used for the test. Since this specimen is aluminum and assumed homogeneous throughout, the primary detected energy, assuming negligible beam divergence of the transmitted beam, is from a bondline on the back surface.

The specimen was bonded to the acoustical couplant holding-tank using Arno double-stick tape which served as a reflecting-scattering layer. It is important to note that multiple interference effects between the specimen front

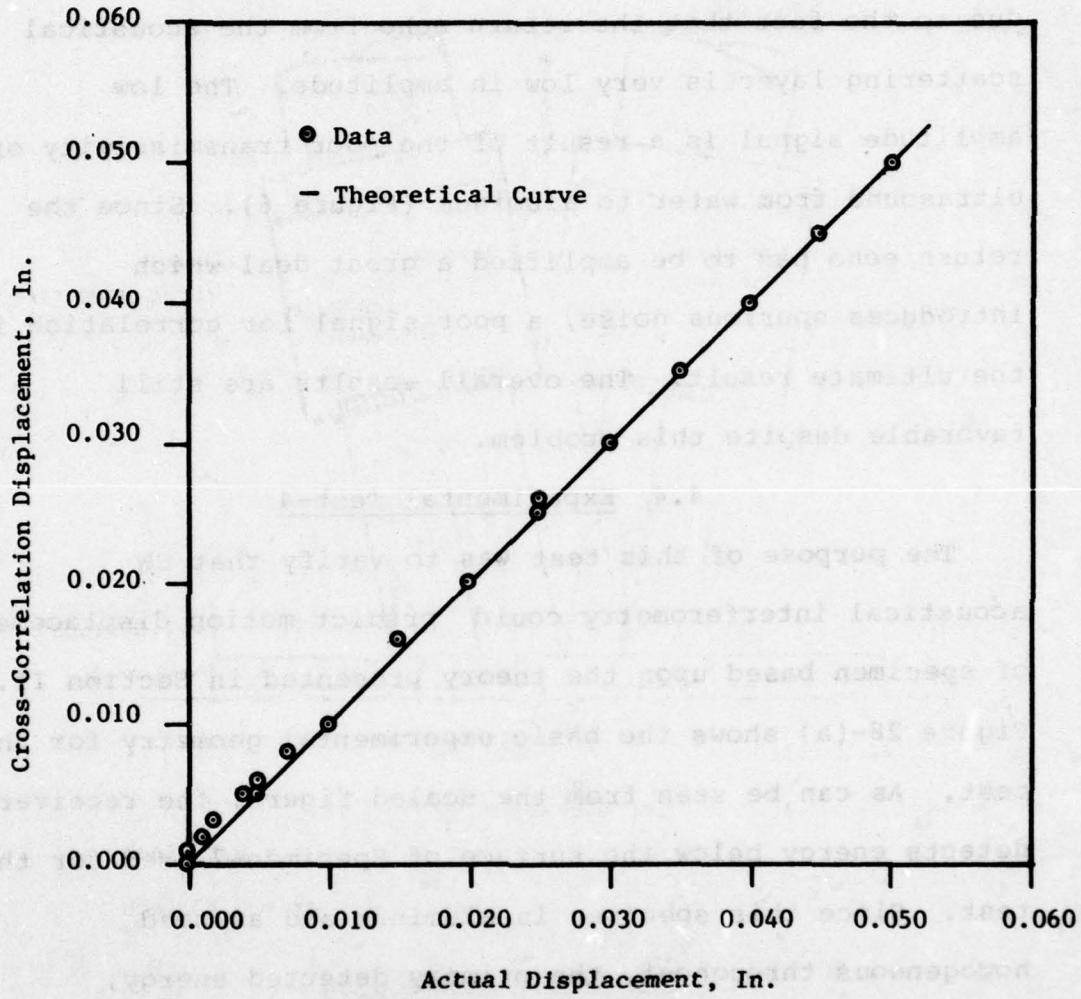

Figure 27. Test-3 Displacement Measured by Cross-Correlation Versus Actual Displacement

(a)

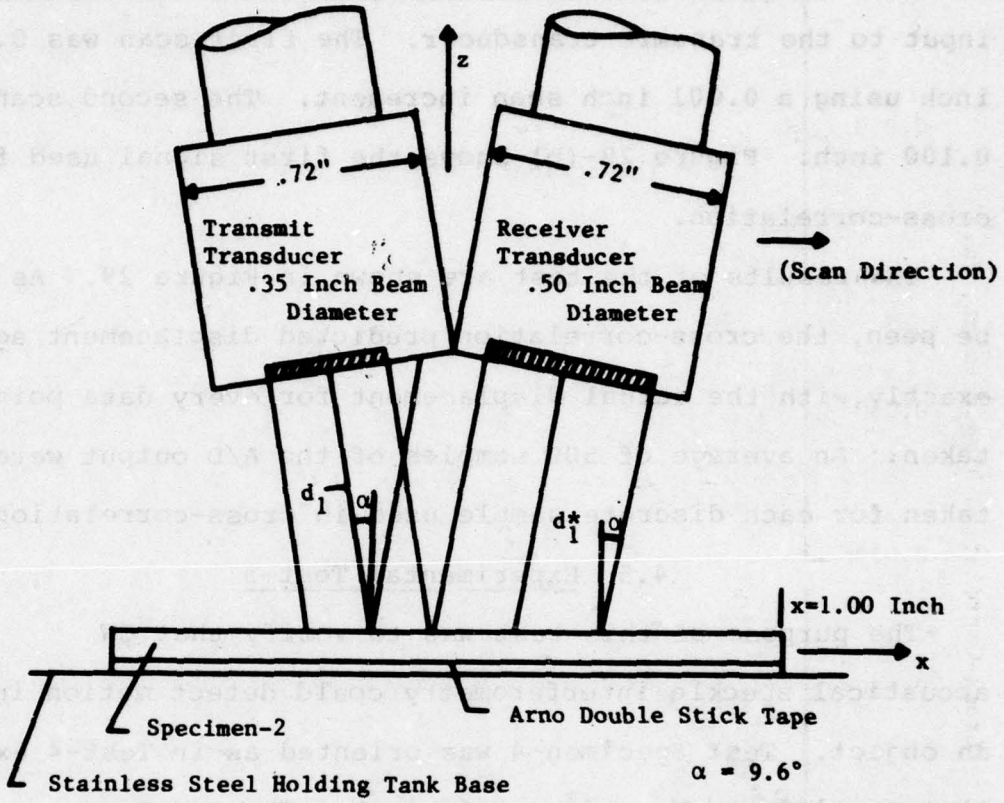

(b)

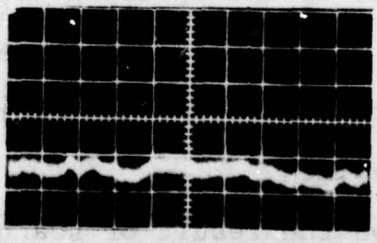

Figure 28. Test-4 Experiment
(a) Test Geometry
(b) First Scan of Specimen

surface and transmit transducer due to multiple reverberations may contribute significantly to the received energy. For the test, an 8.0 volt peak to peak, 3.08 MHz signal was input to the transmit transducer. The first scan was 0.150 inch using a 0.001 inch scan increment. The second scan was 0.100 inch. Figure 28-(b) shows the first signal used for cross-correlation.

The results of the test are shown in Figure 29. As can be seen, the cross-correlation predicted displacement agrees exactly with the actual displacement for every data point taken. An average of 500 samples of the A/D output were taken for each discrete sample used in cross-correlation.

4.5 Experimental Test-5

The purpose of this test was to verify that CW acoustical speckle interferometry could detect motion inside an object. Test Specimen-4 was oriented as in Test-4 except that $\alpha = 10°$ and $d_1 = d_1^* = 0.65$ inch. The scanning was done at 3.08 MHz, 8 volts peak to peak as in Test-4. The grooved surface of the specimen was attached to the double stick tape simulating a definite reflecting-scattering layer, 0.13 inches below the smooth surface of the specimen.

Figure 30 shows the result of scanning 1.00 inch over the surface of the specimen in 0.002 inch increments. A total of 500 discrete samples are shown in which 100 samples

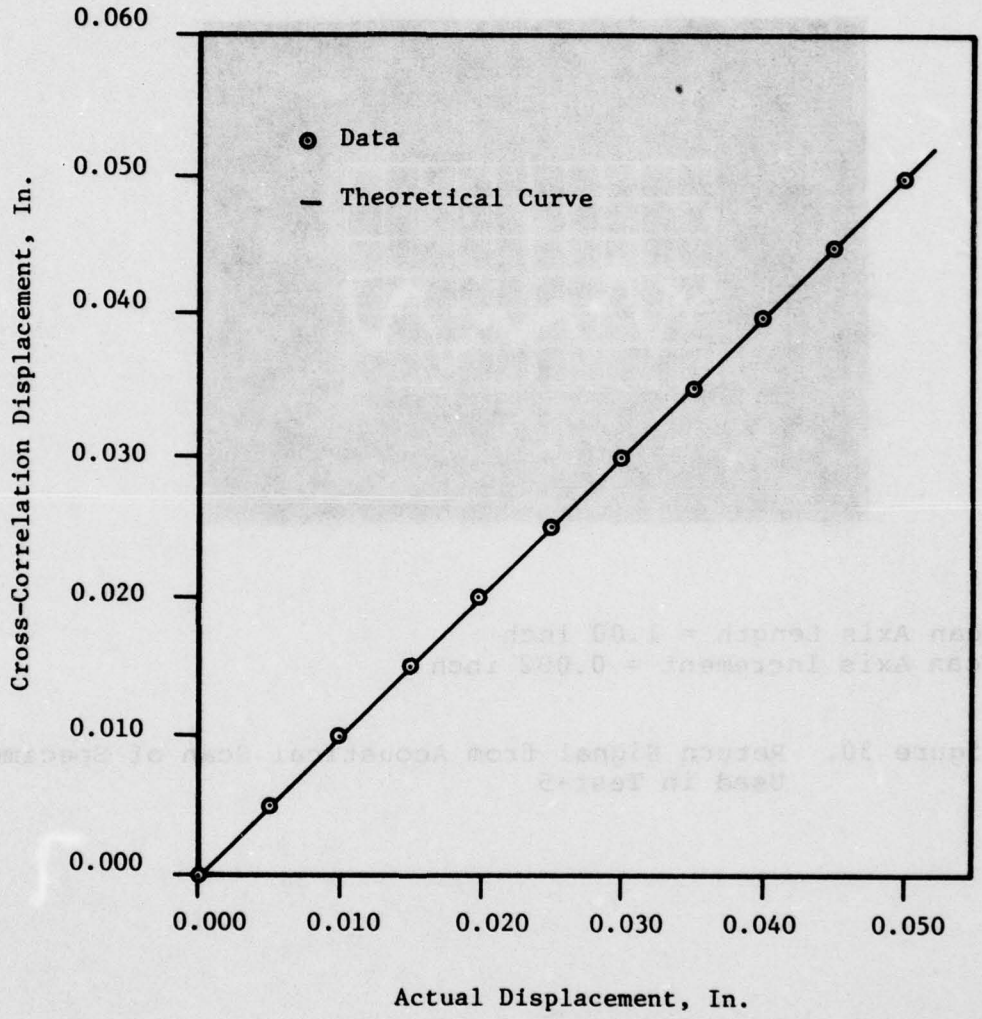

Figure 29. Test-4 Displacement Measured by Cross-Correlation Versus Actual Displacement

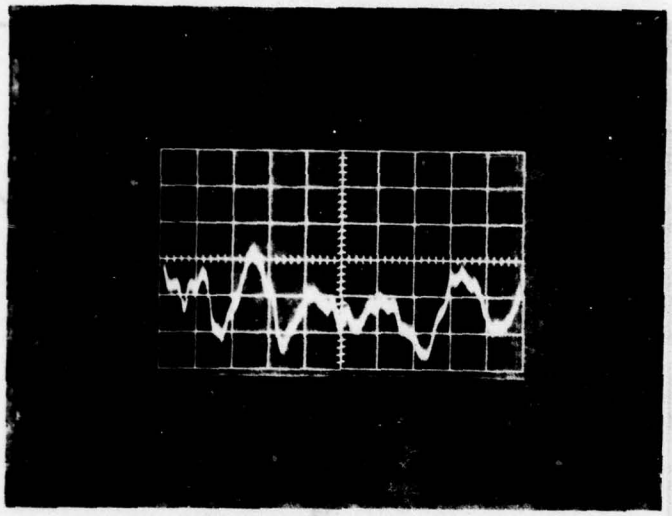

Scan Axis Length = 1.00 inch
Scan Axis Increment = 0.002 inch

Figure 30. Return Signal from Acoustical Scan of Specimen Used in Test-5

per point of the signal were averaged together. As can be seen from this figure, five major maxima and five minima are present indicating the variation in return signal from the scattering layer.

To test the correlation technique, the first scan length was 0.100 inch with 0.001 inch increments between scan points. The second scan length was 0.050 inch. Figure 31 shows the results in which the predicted displacement by cross-correlation agrees exactly with the actual displacement. These results indicate that CW acoustical speckle interferometry can accurately measure displacement of internal points in a solid.

4.6 Experimental Test-6

One of the major problems encountered with pulse-echo scanning is directional sensitivity. If a test specimen as used in Tests 1-3 was translated along the y-axis between the displaced and undeformed x-axis displacements, cross-correlation failed to predict accurate Δx motion. If displacements in the y-axial direction are present, then two-dimensional cross-correlation over the xy-plane is necessary in pulse-echo scanning.

Experimentation showed this not to be the case in CW scanning. This experiment shows a typical case where CW scanning detects only x-axial motion. From the test it is hypothesized that only motion in the plane of the

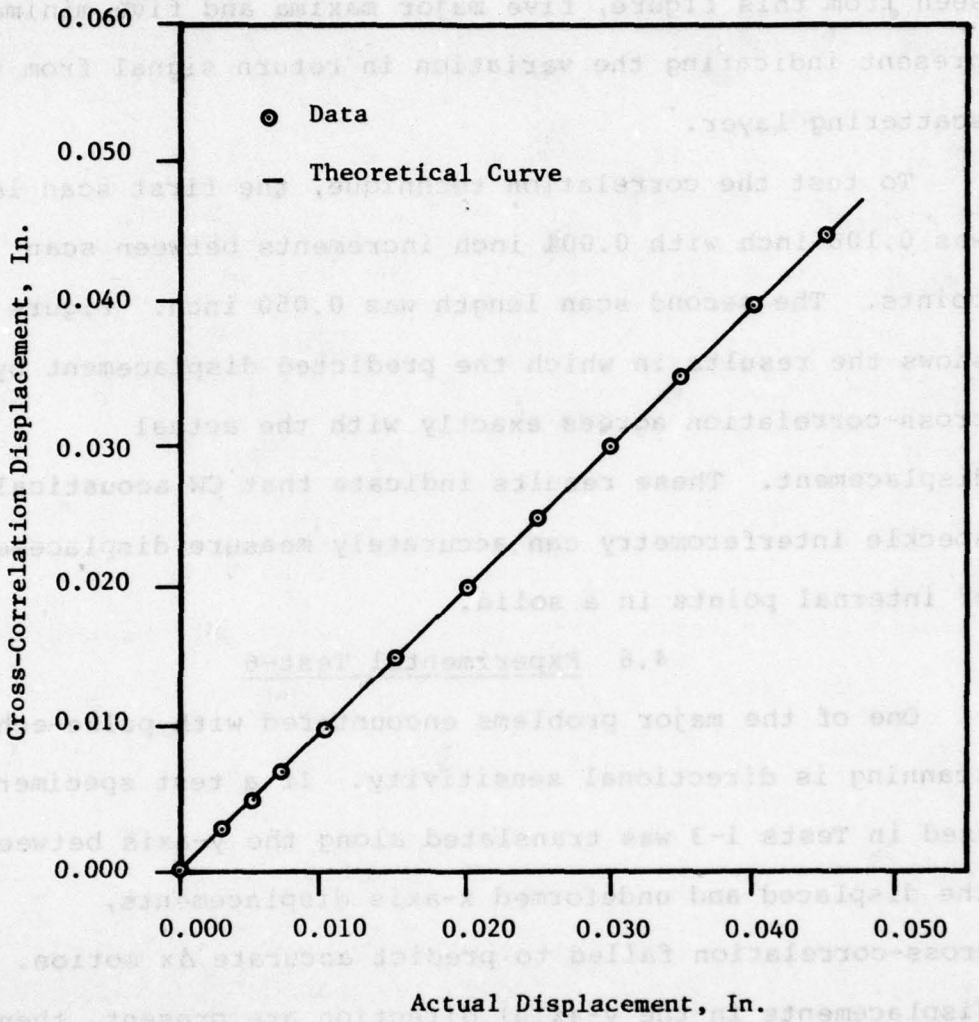

Figure 31. Test-5 Displacement Measured by Cross-Correlation Versus Actual Displacement

transducers (xz-plane) is detected provided that the y-axial displacement is not too large.

The basic test configuration was the same as in Figure 28 except that the slip-cast fused silica (Specimen-3) was used. For the test α = 10.4° and d_1 = 0.78 inch. An 8.0 volt peak to peak load at 3.08 MHz was applied to the transmit transducer. The first scan was made over 0.100 inch using a 0.001 inch scan increment. The second scan was made over 0.050 inch. The transducers were centered over the specimen as before to start the scanning.

In the experiment, the second scan was made a distance Δx, Δy relative to the first scan. Table-2 shows the results of the test. From the data given, it is seen that y axis displacements of $\pm$42% of the beam diameter can be tolerated. This is very important information if an adequate theory can be formulated to predict it. A considerable saving in time would result if all scans could be made in one direction rather than over an entire xy-region. For the experiment, the silica had a uniform smooth surface texture with no indication of being an anistropic scattering surface like Specimen-1. As a point of interest, pulse-echo scanning could not predict motion of the silica due to its surface uniformity which produced very little speckle effect.

TABLE 2

NON-DIRECTIONAL SCAN SENSITIVITY DATA FOR TEST-6

Y-AXIS DISPLACEMENT	ACTUAL X-AXIS DISPLACEMENT				
	.000	.010	.020	.030	.040
.000	----	.010	.020	.030	.039
.001	----	.009	.020	.030	.039
.002	----	.009	.020	.030	.039
.003	----	.009	.020	.030	.038
.004	----	.009	.019	.030	.039
.005	.000	.008	.019	.030	.039
.010	.000	.010	.020	.029	.039
.015	.000	.009	.018	.030	.039
.020	.000	.007	.011	.024	.036
-.001	----	.010	.020	.030	.039
-.002	----	.010	.020	.030	.039
-.003	----	.010	.019	.030	.039
-.004	----	.009	.019	.030	.038
-.005	.000	.009	.019	.030	.038
-.010	.000	.012	.021	.030	.038
-.015	.000	.011	.021	.031	.039
-.020	.000	.014	.022	.033	.041

V. CONCLUSIONS

The basic theory for pulse-echo and continuous wave acoustical speckle interferometry was presented. This theory included the propagation of sound in an LSL interface with a scattering-reflecting layer below the interface. Also the method of scanning and cross-correlation using the square of the difference of two signals was presented. Two separate hardware systems were developed to make displacement predictions using the pulse-echo and continuous wave modes. These systems are very accurate and can make displacement measurements to within $\pm$0.001 inch using an XY-table with a 0.001 inch step increment. XY-tables with a smaller increment could improve these measurements by at least one order of magnitude.

Pulse-echo acoustical interferometry was found to be sensitive to motion in three dimensions which may limit its usefulness since it requires scanning over an area to predict two-dimensional motion. Cross-correlation would have to be achieved in two rather than one dimension which is time consuming from a scanning point of view. Pulse-echo scanning also suffers from poor signal resolution if the scattering layer is very deep below the object.

AD-A067 664 ARMY MISSILE RESEARCH AND DEVELOPMENT COMMAND REDSTO--ETC F/G 20/1
ACOUSTICAL SPECKLE INTERFEROMETRY.(U)
MAR 79 J A SCHAEFFEL

UNCLASSIFIED DRDMI-T-79-39 NL

2 OF 2
ADA
067664

END
DATE
FILMED
6-79
DDC

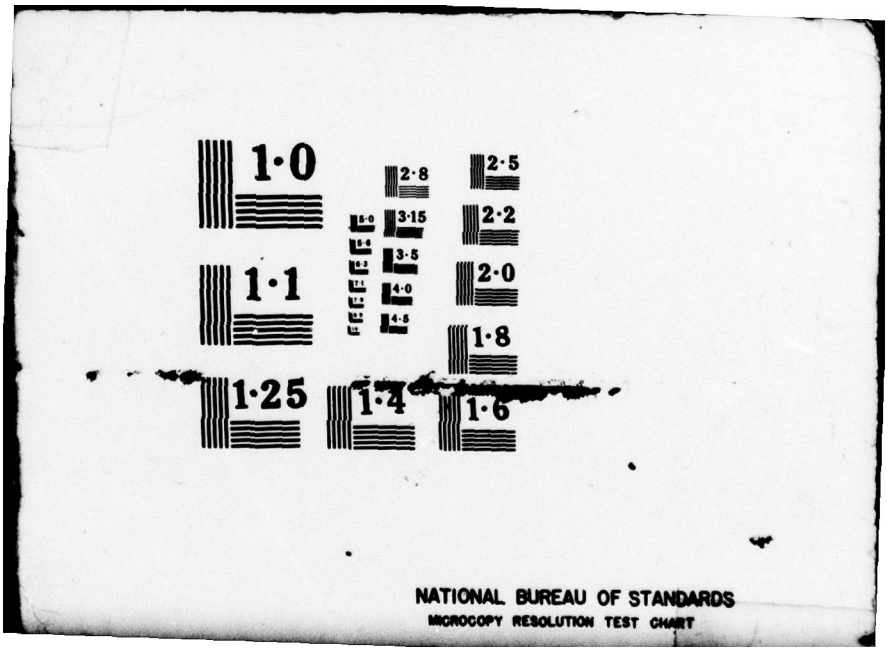
1·0
1·1
1·25
2·8
3·15
3·5
4·0
4·5
1·4
2·5
2·2
2·0
1·8
1·6
NATIONAL BUREAU OF STANDARDS
MICROCOPY RESOLUTION TEST CHART

Continuous wave acoustical speckle interferometry in contrast to pulse-echo scanning was found to be sensitive mainly to motion in two dimensions. With two orthogonal transducer pairs scanning along two orthogonal lines, it may be possible to predict two-dimensional motion using two sets of one-dimensional cross-correlations. This greatly simplifies data acquisition and processing time. Continuous wave scanning gives a very strong signal return from the scattering-reflecting layer which, unlike pulse-echo scanning, is stable in time and can be very accurately measured. This greatly enhances data processing and reduces the cost of the scanning equipment.

There are several problem areas which should be addressed in the future. One area is the analysis of ultrasonic wave propagation in multi-layered scattering-reflecting media. As presented in the theory, the proper positioning of the transducer in CW mode allows for the resolution of ultrasound return echo from any layer in the solid medium. By controlling the position of the receiver transducer, it may be possible to resolve multi-layered reflecting-scattering media. Another area to be addressed is complex geometrical shapes for test objects and their effect on displacement measurements.

REFERENCES

1. Ensminger, D., Ultrasonics-The Low and High-Intensity Applications, Marcel Dekker, Inc., (1973).

2. Hildebrand, B.P., Brenden, B.B., An Introduction to Acoustical Holography, Plenum Press, (1972).

3. Fox, M.D., Ranson, W.F., Griffin, J.R., Pettey, R.H., Acoustical Holography, Vol. 5, Editor P.S. Green, Plenum Press, (1973).

4. Ranson, W.F., "Use of Holographic Interferometry to Determine the Surface Displacement Components of a Deformed Body", Ph.D. Thesis, Department of Theoretical and Applied Mechanics, University of Illinois, Urbana, Illinois, (August, 1971).

5. Kinariwala, V.R., "Determination of Surface Stresses Using Speckle Interferometry", M.S. Thesis, Department of Mechanical Engineering, Auburn University, Auburn, Alabama, (March, 1976).

6. Goldman, R., Ultrasonic Technology, Reinhold Publishing Corp., (1962).

7. Shaw, W.A., Smith, F.S., Strength of Materials, Class Notes, Department of Mechanical Engineering, Auburn University, Auburn, Alabama, (1968).

8. Wills, A.P., Vector Analysis With An Introduction to Tensor Analysis, Dover Publications, Inc., (1958).

9. Brekhovskikh, L.M., Waves In Layered Media, Academic Press, New York, (1960).

10. Betts, J.A., Signal Processing, Modulation and Noise, American Elsevier Publishing Company, Inc., New York, (1971).

```
      RETURN
      END
      SUBROUTINE CORR(ID,N,M,IC)
      DIMENSION ID(2,500)
      S2=10E20
      INM=0
      ICNM=N-M
      DO 2 I=0,ICNM,1
      S=0.
      DO 1 J=1,M,1
      S1=FLOAT(ID(2,J)-ID(1,I+J))
1     S=S+S1*S1
      IF(S.LT.S2) INM=I
      IF(S.LT.S2) S2=S
2     CONTINUE
      D=.001*FLOAT(INM*IC)
      WRITE(5,3) D,S2
3     FORMAT(' DISPLACEMENT=',F10.3,5X,'CORRELATION=',E12.5)
      RETURN
      END
      SUBROUTINE PLOT(I,ID,NP)
      DIMENSION ID(2,500)
1     ITEST=IPEEK('177570)
      IF(ITEST.NE.0) GOTO 1
2     CALL IPOKE('170410,'1)
      CALL IPOKE('170410,'0)
      DO 3 J=1,NP,1
      IP=ID(I,J)
      CALL IPOKE('170414,IP)
3     CALL IPOKE('170414,'0)
      ITEST=IPEEK('177570)
      IF(ITEST.EQ.0) GOTO 2
      RETURN
      END
      SUBROUTINE YADV(IS,IR)
C-----IS=NO. STEPS (+=FWD,-=REV)
C-----IR=ADVANCE RATE OF STAGE
      X=0.
      IF(IS.GT.0) GOTO 3
      IP=IABS(IS)
      DO 2 I=1,IP,1
      CALL IPOKE('167772,'020000)
      DO 7 K=1,IR,1
7     Y=SIN(X)
      CALL IPOKE('167772,'000000)
      DO 1 J=1,IR,1
```

```
1       Y=SIN(X)
2       CONTINUE
        GOTO 6
3       CONTINUE
        DO 5 II=1,IS,1
        CALL IPOKE('167772,'010000)
        DO 8 KK=1,IR,1
8       Y=SIN(X)
        CALL IPOKE('167772,'000000)
        DO 4 JJ=1,IR,1
4       Y=SIN(X)
5       CONTINUE
6       CONTINUE
        RETURN
        END
        SUBROUTINE XADV(IS,IR)
C-----IS=NO. STEPS (+=FWD,-=REV)
C-----IR=ADVANCE RATE OF STAGE
        X=0.
        IF(IS.GT.0) GOTO 3
        IP=IABS(IS)
        DO 2 I=1,IP,1
        CALL IPOKE('167772,'100000)
        DO 7 K=1,IR,1
7       Y=SIN(X)
        CALL IPOKE('167772,'000000)
        DO 1 J=1,IR,1
1       Y=SIN(X)
2       CONTINUE
        GOTO 6
3       CONTINUE
        DO 5 II=1,IS,1
        CALL IPOKE('167772,'040000)
        DO 8 KK=1,IR,1
8       Y=SIN(X)
        CALL IPOKE('167772,'000000)
        DO 4 JJ=1,IR,1
4       Y=SIN(X)
5       CONTINUE
6       CONTINUE
        RETURN
        END
*
```

DISTRIBUTION

	No. of Copies
Defense Metals Information Center Battelle Memorial Institute 505 King Avenue Columbus, Ohio 43201	1
Defense Documentation Center Cameron Station Alexandria, Virginia 22314	12
Commander US Army Foreign Science and Technology Center Attn: DRXST-SD3 220 Seventh Street, NE Charlottesville, Virginia 22901	1
Office of Chief of Research and Development Department of the Army Attn: DARD-ARS-P Washington, D. C. 20301	1
Commander US Army Electronics Command Attn: DRSEL-PA-P -CT-DT -PP, Mr. Sulkolove Fort Monmouth, New Jersey 07703	1 1 1
Commander US Army Natick Laboratories Kansas Street Attn: STSNLT-EQR Natick, Massachusetts 01760	1
Commander US Army Mobility Equipment Research and Development Center Fort Belvoir, Virginia 22060	1
Director USA Mobility Equipment Research and Development Center Coating and Chemical Laboratory Attn: STSFB-CL Aberdeen Proving Ground, Maryland 21005	1
Commander Edgewood Arsenal Attn: SAREA-TS-A Aberdeen Proving Ground, Maryland 21010	1
Commander Picatinny Arsenal Attn: SAPPA-TS-S, Mr. M. Costello Dover, New Jersey 07801	1
Commander Rock Island Arsenal Research and Development Attn: 9320 Rock Island, Illinois 61201	1
Commander Watervliet Arsenal Watervliet, New York 12189	1
Commander US Army Aviation Systems Command Attn: DRSAV-EE -MT, Mr. Vollmer St. Louis, Missouri 63166	1 1
Commander US Army Aeronautical Depot Maintenance Center (Mail Stop) Corpus Christi, Texas 78403	1
Commander US Army Test and Evaluation Command Attn: DRSTE-RA Aberdeen Proving Ground, Maryland 21005	1
Commander Attn: STEAP-MT Aberdeen Proving Ground, Maryland 21005	1
Chief Bureau of Naval Weapons Department of the Navy Washington, D. C. 20390	1
Chief Bureau of Ships Department of the Navy Washington, D. C. 20315	1
Naval Research Laboratory Attn: Dr. M. M. Krafft Code 8430 Washington, D. C. 20375	1
Commander Wright Air Development Division Attn: ASRC Wright-Patterson AFB, Ohio 45433	1
Director Air Force Materiel Laboratory Attn: AFML-DO-Library Wright-Patterson AFB, Ohio 45433	1
Director, Army Materials and Mechanics Research Center Attn: DRXMR-PL -MT, Mr. Farrow Watertown, Massachusetts 02172	1 1
Commander White Sands Missile Range Attn: STEWS-AD-L White Sands Missile Range, New Mexico 88002	1
Deputy Commander US Army Nuclear Agency Attn: MONA-ZB Fort Bliss, Texas 79916	1
Jet Propulsion Laboratory California Institute of Technology Attn: Library/Acquisitions 111-113 4800 Oak Grove Drive Pasadena, California 91103	1
Sandia Laboratories Attn: Library P. O. Box 969 Livermore, California 94550	1
Commander US Army Air Defense School Attn: ATSA-CD-MM Fort Bliss, Texas 79916	1

	No. of Copies
Technical Library Naval Ordnance Station Indian Head, Maryland 20640	1
Commander US Army Materiel Development and Readiness Command Attn: DRCMT Washington, D. C. 20315	1
Headquarters SAC/NRI (Stinfo Library) Offutt Air Force Base, Nebraska 68113	1
Commander Rock Island Arsenal Attn: SARRI-RLPL-Technical Library Rock Island, Illinois 61201	1
Commander (Code 233) Naval Weapons Center Attn: Library Division China Lake, California 93555	1
Department of the Army US Army Research Office Attn: Information Processing Office P. O. Box 12211 Research Triangle Park, North Carolina 27709	1
ADTC (DLDSL) Eglin Air Force Base, Florida 32542	1
University of California Los Alamos Scientific Laboratory Attn: Reports Library P. O. Box 1663 Los Alamos, New Mexico 87545	1
Commander US Army Materiel Development and Readiness Command Attn: DRCRD DRCDL 5001 Eisenhower Avenue Alexandria, Virginia 22333	1 1
Director Defense Advanced Research Projects Agency 1400 Wilson Boulevard Arlington, VA 22209	1
DRSMI-LP, Mr. Voigt	1
DRDMI-K	1
-T, Dr. Kobler	1
-TL, Mr. Lewis	1
-TLA, Mr. Pettey	1
-TLA, Dr. Mullinix	1
Mr. Scheeffel	80
-EA	2
-EAA	2
-EAS	1
-EAM	1
-EAP	1
-EAR	1
-EAT	3
-ICSB	1
-TBD	3
-TI (Record Set)	1
(Reference Copy)	1

	No. of Copies
Commander US Army Research Office Attn: DRXRO-PH, Dr. R. Lontz P.O. Box 12211 Research Triangle Park, NC 27709	2
US Army Research and Standardization Group (Europe) Attn: DRXSN-E-RX, Dr. Alfred K. Nedoluha Box 65 FPO New York 09510	2
Headquarters Department of the Army Office of the DCS for Research Development and Acquisition Room 3A474, The Pentagon Attn: DAMA-ARZ Washington, DC 20310	2
US Army Material Systems Analysis Activity Attn: DRXSY-MP Aberdeen Proving Ground, MD 21005	1